An Integration of Planar Cavity-Backed Antenna with Artificial Magnetic Conductor in the Application of 2.4 GHz WBAN Application

By

Abu Hena Murshed, MSc Eng

20METE012F

A thesis submitted in partial fulfillment of the requirements for the degree of MASTER of SCIENCE in Electronics & Telecommunication Engineering

Department of Electronics & Telecommunication Engineering

CHITTAGONG UNIVERSITY OF ENGINEERING AND TECHNOLOGY

AUGUST 2023

Declaration

I hereby declare that the work contained in this Thesis has not been previously submitted to meet the requirements for an award at this or any other higher education institution. To the best of my knowledge and belief, the Thesis contains no material previously published or written by another person except where due reference is cited. Furthermore, the Thesis complies with PLAGIARISM and ACADEMIC INTEGRITY regulation of CUET.

Abu Hena Murshed
20METE012F
Department of Electronics & Telecommunication Engineering
Chittagong University of Engineering & Technology (CUET)

Dedication

To my amazing friends and critics

and

To my beloved family members for being infinitely supportive

List of Publications

Journal Article

- Publication 1: **A.H. Murshed**, et.al, "A half-mode cavity-backed hybrid array antenna using substrate integrated waveguide (SIW) technology" in *IEEE Transactions on Antennas and Propagation*, vol. 71, no.1, pp.169-179, Jan. 2023. DOI: 10.1109/TAP.2022.3218959.
- Publication 2: M. A. Hossain, **A. H. Murshed**, M. A. Rahman, E. Nishiyama, and I. Toyoda, "A gain enhanced linear polarization switchable array antenna with switching diodes," *Int. J. RF Microw. Comput.-Aided Eng*., vol. 32, no. 10, pp. 1–9, Jun. 2022. DOI: 10.1002/mmce.23291.
- Publication 3: M. A. Hossain, **A. H. Murshed**, M. A. Rahman, E. Nishiyama, and I. Toyoda, "A novel dual-band slot-ring array antenna using both-sided MIC technology for polarization detection," *Int. J. RF Microw. Comput.-Aided Eng*, vol. 13, no. 11, Aug. 2022. DOI: 10.1002/mmce.23373.
- Publication 4: P. Chowdhury, N. Chakma, **A. H. Murshed**, M. A. Hossain, and Q. D. Hossain, "An improved 2×2 array antenna using both-sided microwave integrated circuit technology for circular polarization," *Int. J. Electr. Comput. Eng*., vol. 13, no. 1, pp. 619–628, Feb. 2023. DOI: 10.11591/ijece.v13i1.pp619-628.
- Publication 5: **A. H. Murshed,** M. A. Hossain, N. K. Kiem, N. H. Hai, E. Nishiyama, and I. Toyoda, "Simple Integration of Cavity-Backed Antenna with Patch Antenna for Developing Hybrid Antenna Using SIW Technology" submitted in *Int. J. of Antennas and Propag*.

Approval by the Supervisor

This is to certify that Abu Hena Murshed has carried out this research work under my supervision, and that he has fulfilled the relevant Academic Ordinance of the Chittagong University of Engineering and Technology, so that he is qualified to submit the following Thesis in the application for the degree of MASTER of SCIENCE in Electronics & Telecommunication Engineering. Furthermore, the Thesis complies with the PLAGIARISM and ACADEMIC INTEGRITY regulation of CUET.

Prof. Dr. Md. Azad Hossain

Head of department

Department of Electronics & Telecommunication Engineering

Chittagong University of Engineering & Technology

Acknowledgement

I would like to unearth my deepest gratitude to Almighty Allah, the supreme omnipotent of this whole universe to give me the ability, strength, patience and time to complete this thesis successfully.

I wish to express my heartiest and sincere gratitude to my venerated supervisor Dr. Md. Azad Hossain, Professor, Dept. of ETE, Chittagong University of Engineering and Technology (CUET), for his continuous supervision, inspiration, insightful guidance, and helpful instructions throughout the thesis work. He has tried his best to provide all the necessary support in every step of this work; without that it would have been impossible to complete this thesis work. I would like to convey my deepest appreciation and gratitude to Dr. Ichihiko Toyoda, Professor, Dept. of EEE, Saga University, Japan, not only for his research expertise and amenable attitude but also for his valuable advice and all kinds of necessary support. Additionally, thanks to Dr. Nguyen Hoang Hai, Professor, Faculty of Communication Engineering, Hanoi University of Science and Technology (HUST), Vietnam, for providing support for the experimental validation of the antenna.

Special thanks to directorate of planning & development (P&D) of CUET for carrying out a project by the name of 'Development of Chittagong University of Engineering & Technology', under which I was granted a scholarship. This scholarship facilitates me to earn an MSc in engineering degree in the Dept. of ETE, CUET. I take the privilege to express my special gratitude to the scholars for their valuable advice, suggestions and inspirations. Finally, I am also grateful to my parents, and family members for their constant love, support, and encouragement that are a continuous source of joy and strength.

Abstract

A high-gain array antenna is proposed using cavity-backed technology with the help of Substrate Integrated Waveguide Technology. The joint combination of both patch and the cavity-backed antenna is also known as a hybrid combination. Such types of antennas allow bandwidth enhancement and further division of patches to allow high gain and low cross-polarization behaviour. The whole patch antenna is further divided and based on the number of array elements in the patch, four array antenna cases have been proposed. A comprehensive investigation of them is presented. The proposed antenna operates at Ku-band, showing linearly polarized wave in TE_{101} mode and this hybrid combination provides several advantages. First, it has the advantages of a cavity-backed antenna and the conventional slot antenna. Second, an antenna is more compact. Third, it contains a much simpler matching network. In addition, being a member of the planner waveguide family, the proposed antenna also possesses a low profile and allows easy integration with the planner circuit. An exact representation of parameters of all antennas that have emerged during the designing course helps to grasp the sense of designing such kinds of hybrid array antenna of planner waveguide technology. Later, the proposed antenna is verified experimentally and exhibits a satisfying agreement with the data found during numerical simulation. The antennae's simulated parameters were investigated with the help of CST (computer simulation technology) and HFSS (high frequency structure simulator) simulation software in microwave momentum mode.

বিমূর্ত

এই অভিসন্দর্ভে দুটো উচ্চ গেইন সম্পন্ন এ্যারে এন্টেনা প্রস্তাবিত করা হয়েছে যার মধ্যে একটি ক্যাভিটি-ব্যাক্ড প্রযুক্তি এবং অন্যটি বোথ সাইডেড এমআইসি প্রযুক্তির মাধ্যমে। হাইব্রিড প্রযুক্তি হচ্ছে প্যাচ এন্টেনা ও ক্যাভিটি-ব্যাক্ড এন্টেনার মিশ্রণ। এই ধরনের সমাবেশ এন্টেনার ব্যান্ডউইথ বৃদ্ধিকরন এবং প্যাচকে আরও ছোট অংশে বিভক্ত করার মাধ্যমে এন্টেনার গেইন বৃদ্ধি করা, এবং ক্রস পোলারাইজেশন কমিয়ে ফেলা সম্ভব। পুরো প্যাচকে আরও বিভক্ত করার মাধ্যমে এবং কত অংশে বিভক্ত করা হয়েছে তার উপর ভিত্তি করে চার ধরনের এন্টেনা প্রস্তাবিত করা হয়েছে এবং তাদের উপর চালানো ব্যাপক বিশ্লেষণ উপস্থাপনা করা হয়েছে। প্রস্তাবিত এন্টেনাটির কিছু সুবিধা রয়েছে যা Ku-ব্যান্ডে কার্যকম করে এবং TE_{101} এই মোডের মাধ্যমে লিনিয়ার পোলারাইজেশন ওয়েভ নির্গত করে। প্রথমত, এটির রয়েছে ক্যাভিটি-ব্যাক্ড ও সমসাময়িক স্লট এন্টেনার মিশ্রণ। দ্বিতীয়ত, এটির রয়েছে খুবই ছোট সাইজ। তৃতীয়ত এটির রয়েছে সহজতর ম্যাচিং নেটওয়ার্ক। এছাড়াও ওয়েভগাইড পরিবারের সদস্য হওয়ার কারনে এটিতে রয়েছে ছোট প্রোফাইল এবং প্ল্যানার সার্কিটে সহজভাবে ব্যাবহার করা যায়। যথাযথ বিশ্লেষণের মাধ্যমে যেটা এই প্রবন্ধে উপস্থাপনা করা হয়েছে, কেনো এই ধরনের এন্টেনা ডিজাইন করা প্রয়োজন সেটার গুরুত্ব উপলব্ধি করা সম্ভব। পরবর্তীতে এন্টেনাটিকে ফ্যাব্রিকেটেড করার পর মাইক্রোওয়েভ চ্যাম্বারে পরীক্ষার মাধ্যমে এর কার্যকারিতা বিচার করা হয়েছে। এন্টেনা দুটিকে সিমুলেশন এর জন্য সিএসটি এবং এডিএস, এই দুইটি সফটওয়্যার কে ব্যাবহার করা হয়েছে।

Table of Contents

List of Figures

List of Tables

Table No. **Table Caption** **Page No.**

Nomenclature

VSWR	Voltage Standing Wave Ratio
IEEE	Institute of Electrical and Electronic Engineers
PFD	Power Flux Density
RC	Reflection Coefficient
BW	Bandwidth
HPBW	Half-power Beam Width
FNBW	First-null Beam Width
2D	2-Dimensional
SIW	Substrate Integrated Waveguide
HMSIW	Half Mode Substrate Integrated Waveguide
FTBR	Front to back ratio.
MIC	Microwave Integrated Circuit
PBG	Photonic Bandgap
EBG	Electronic Bandgap
CST	Computer Simulation Technology
RF	Radio Frequency
TE	Transverse Electric
TM	Transverse Magnetic
MIMO	Multiple Input Multiple Output
5G	Fifth Generation
DL	Dielectric Length
MPA	Microstrip Patch Antenna
RWG	Rectangular Waveguide
HFSS	High Frequency Structure Simulator
SLL	Sidelobe level
SRR	Split Ring Resonator

Chapter 1: INTRODUCTION

1.1 BACKGROUND

At the beginning of the century, wireless communications began a long road full of prosperous progress. Since Marconi's proposals today, the technologies used for wireless communications have progressed very fast. These advances have always had as its purpose the low power consumption, miniaturization of components, and, above all, maximum efficiency. With the advent of transistors, circuits have achieved high performance, and current receivers have widely reduced their size. The transistors have enabled many applications such as amplifiers, oscillators, mixers, among others. Without a doubt, this nonlinear device allows a wide range of important applications to the development of wireless communications.

Nowadays, in microwave communications, receivers have achieved a great reduction of their size, maintaining their efficiency. This is due to the use of the transistor and other technologies that complement each other. One of them is the use of microstrip technology to design passive circuits. Microstrip is widely used due to its compact size and easy integration. But with frequency increasing as an open structure, a microstrip circuit shows undesirable radiation. To solve these kinds of problems we can use substrate integrated waveguide (SIW) technology.

The SIW technology is important because any non-planar waveguide-like structure (including classical rectangular waveguide) can be synthesized into planar form, seamlessly integrated with conventional printed planar circuits (including transitions, active components, and antennas). This is one of the major advantages of SIW technology because allow us to fabricate a complete circuit in

planar form. Moreover, it is possible to mount one or more chips on the same substrate, reducing losses and parasitic. Using SIW technology, one can optimize an antenna structure and integrate it with different components.

1.2 MOTIVATION AND OBJECTIVES

SIW antennas have recently sparked a lot of interest. Due to their simplicity and compatibility with printed-circuit board technology. The planar waveguides are frequently employed in the microwave frequency spectrum. By cutting slots and or dividing along aperture they can be converted into antenna. Such types of antennas can enhance broadside radiation and curtail sidelobe level. The planar cavity-backed antenna can be made in action just characterizing it like a rectangular, square, circular, triangular or any other shape based on its application to meet its requirement. The row of cylinders in SIW act as wall to prevent leakage. However, metallic cylinders contribute to a high *Q*-factor resulting in narrow BW response. Normally, it could be made up of three-layers (or more depending upon the requirements) such as ground, substrate and patch layer which makes it easier to fabricate, design, analysis, low cost, lightweight etc. Apart from, it can be made as a single unit or can be made as a part of the array antenna. Despite having such disadvantages, low BW and large size, some steps can be taken to outweigh its limitations. For the past few decades, much research on SIW-antennas have been accomplished to grapple with its problem and to make it more promising candidate in the field of microwave communication while adding some technique on it.

RESEARCH APPROACH

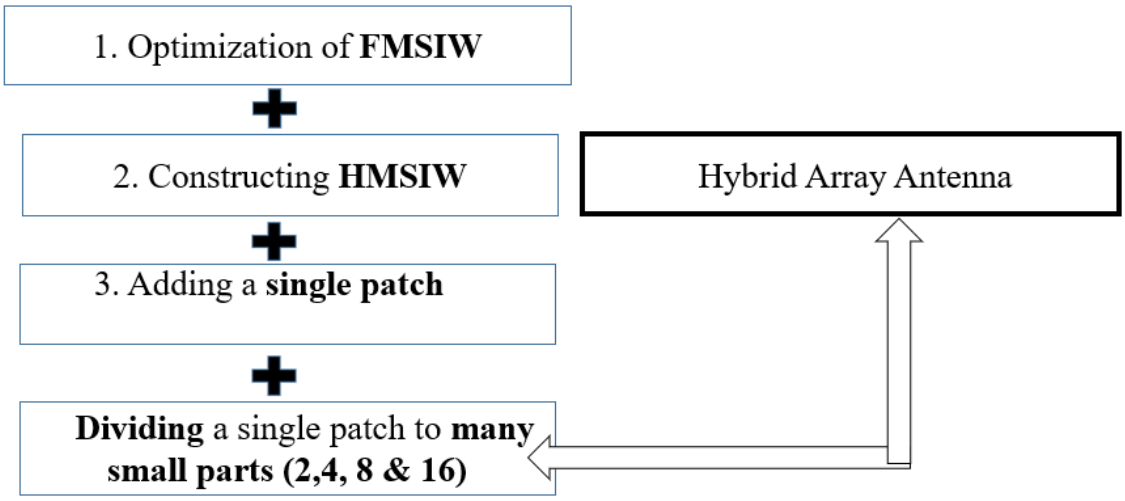

1.3 CONTRIBUTION OF THE THESIS

This thesis has addressed some of the inborn problems of typical microstrip antenna such as high sidelobe level (SLL), low bandwidth, low gain, and also pays attention to size reduction. To resolve, some techniques are employed, such as the planer waveguide technology to reduce SLL, half-mode for reducing size, multi-resonator for BW, and parasitic array for increased gain. These different techniques have been employed in one single substrate layer and a meticulous representation along with experimental validation will help the reader to realize the necessity of such arrangement to solve the inborn problems. The use of a cavity-backed antenna with a patch antenna allows to achieve a new combination can be called as Hybrid combination. This has been done to attain bandwidth fidelity, capability of integrating in planar circuit, and to reduce antennas backward radiation.

1.4 THESIS OUTLINE

The thesis is comprised of 5 chapters. The contents of each chapter are arranged as follows:

Chapter 1 contains the background and motivation of the proposed work. Focus of this thesis alongside with research contribution is also discussed briefly by explaining the works and outcomes of this study.

Chapter 2 discusses the literature review of the previously published antenna and their drawbacks.

Chapter 3 discusses the fundamentals of the microstrip antenna, how are they consists of, methods of analysis, advantages and disadvantages, polarization and feeding techniques. It also gives a general idea about substrate integrated waveguide (SIW) technology and how it works. Moreover, a short overview on artificial magnetic conductor, is depicted in this chapter.

Chapter 4 presents a hybrid array antenna which is joint combination of both patch antenna and planner cavity-backed antenna. Four different types of array antenna are presented, and meticulous theoretical analysis is presented. Further providing the experimental data of the antennas are investigated and simulation results are verified.

Chapter 5 discusses the conclusions of the thesis and provides directions of the future work for further improvement of the proposed antennas.

Chapter 2: LITERATURE REVIEW

2.1 HISTORICAL BACKGROUND

As of late, society has been witnessing the rapid development of wireless technology where microwave communication systems demand microstrip antenna [1-4] as they ensure the feasibility of design, low profile, low cost, and numerous conducive characteristics. The cavity-backed antenna has recently drawn significant attention among researchers and further research is ongoing as it can provide high gain, high radiation efficiency, etc. Its advantages of ruling out backward radiation and the ability to curb the surface wave radiation make the cavity-backed antenna better than that of conventional patch and slot antennas [5-8].

Moreover, the technology for employing microwave circuits, named SIW technology, has broken new ground in microwave engineering. It has been very popular as it acts like a conventional metallic waveguide on a single substrate and provides a couple of mesmerizing characteristics like the ability to use in planar circuits, low conductor loss, and high-quality factor [9]. The cavity-backed antenna also can be backed by SIW technology, and some low-profile slot cavity-backed antenna are reported in [10-12]. Half-mode SIW (HMSIW) is being designed nowadays for microwave components as proposed in [13-14]. By determining a quasi-magnetic wall and dividing it alongside the wall, SIW can be divided into two or more parts. The HMSIW or quarter-mode SIW (QMSIW) can emerge in this way [13-19].

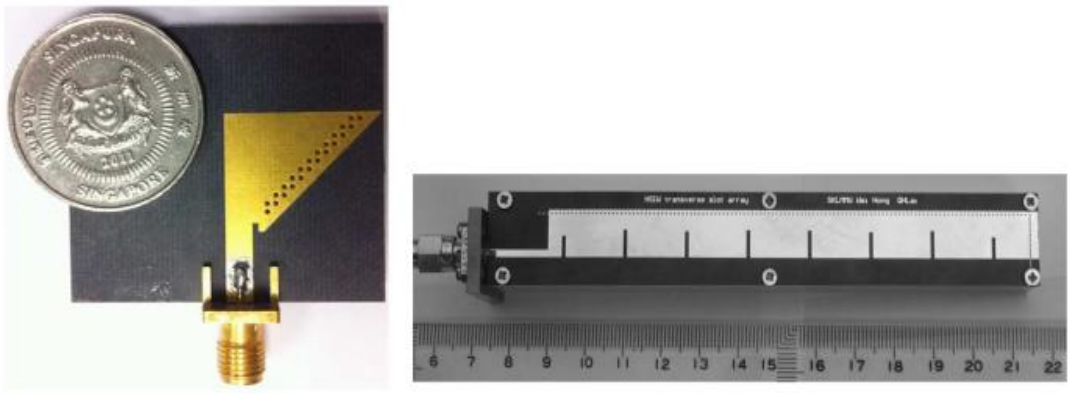

(a) (b)

Fig. 2.1. (a) Prototype of the fabricated QMSIW antenna [19] and (b) Photographs of the HMSIW-fed transverse resonant slot array antennas [16].

The emerged HMSIW can accommodate almost same the electric field as for original SIW, and leaky-wave radiation can be obtained from HMSIW through its dielectric aperture as designed in [15-18]. The HMSIW slot array antenna is also proposed by many researchers as designed in [20], where SIW-backed slot array antenna is presented for satellite communication.

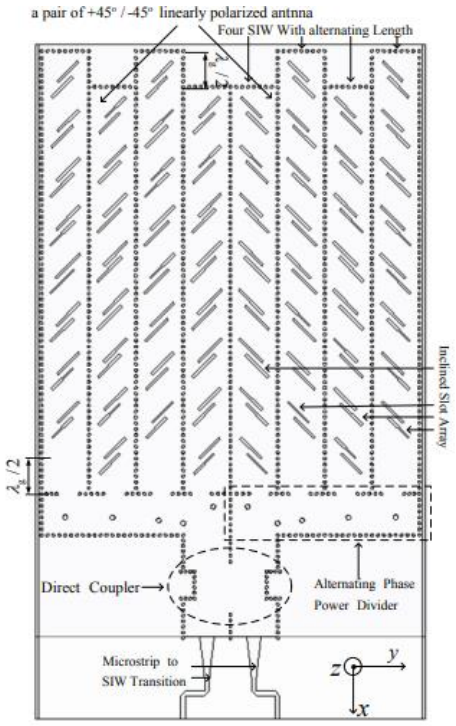

Fig. 2.2. The SIW Circularly Polarized Antenna Geometry [20]

An HMSIW transverse slot array antenna is proposed to operate at X- and Ka-band. A cavity-backed planner slot array antenna combined grounded coplanar waveguide is also proposed in [10] working at X-band. A patch array antenna is also suggested using cavity-backed SIW technology, where the antenna obtained a net gain of 7.8 dBi [21-22]. The antenna with the parasitic patch elements is considered to be a novel technique for improving the antenna's net gain and bandwidth (BW) as proposed in [23-26].

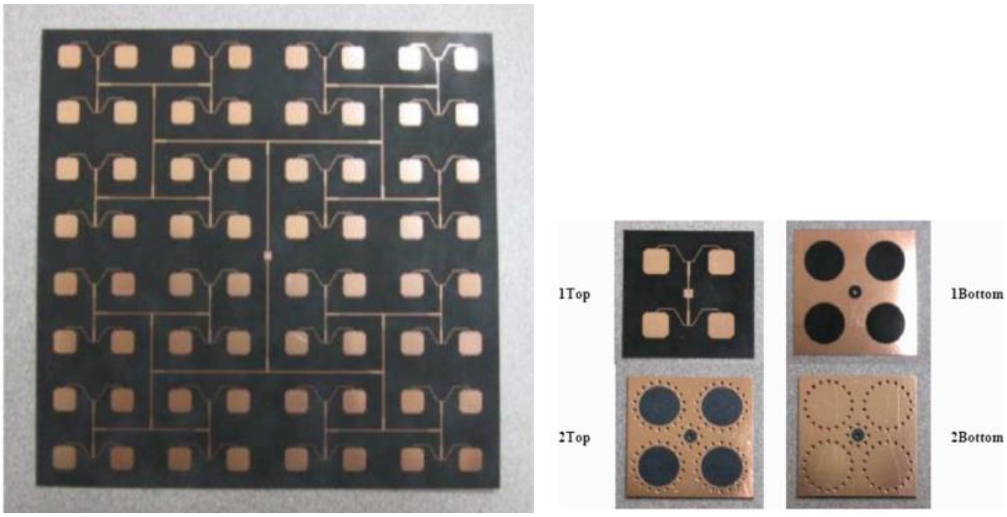

(a) (b)

Fig. 2.3. (a) Picture of the fabricated SIW cavity-backed patch arrays, 8 × 8 arrays (b) Photograph of the fabricated structure depicting the top and bottom artworks of the microstrip substrate, 1Top and 1Bottom, and the cavity substrate, 2Top and 2bottom.

In [24], an antenna consists of two parasitic elements, and one of them helps to achieve high gain, whereas the other one achieves wide BW. Those elements were stacked over each other, and the relative height between those elements also determined the net gain, BW, and impedance matching. However, this relative height increases antenna thickness. In [25], a thick substrate layer helps to reduce antenna thickness between the parasitic and fed patch in [25], where the fine-tuning distance between the patch and its shape determines wide BW and gain. Moreover, this insertion of extra substrate helps to reduce thickness by 30%. Then a thin layer of substrate is proposed in two layers of the high gain antenna to

reduce further thickness where the parasitic elements play a vital role in improving gain [26]. These techniques meet the desired requirement; however, inversely also increase the magnitude of antennas' overall thickness.

Subsequently, in [27] and [28] patch was also chosen to address the requirements. In [27], a loaded meta-surface antenna (MA) comprises of a square patch is proposed to achieve stable broadside radiation by suppressing higher-order modes in a multiport antenna system.

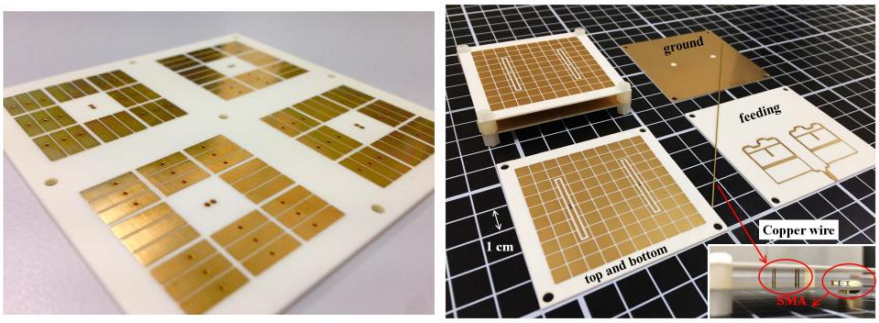

(a) (b)

Fig. 2.4. (a) Photograph of the fabricated sample of the meta-surfaces [27] and (b) Photographs of the antenna prototype. The long copper wire is chopped into segments to connect the dipole on the top and the balun at the bottom [28].

Furthermore, the patch acted as a second resonator and contributed to an escalation of BW. In [28], a very similar patch for a triple-mode low-profile MA is proposed, where an accurate and fast analysis was carried out on it by an impedance sheet model using characteristics mode analysis (CMA) [28]. Note that BW escalation was done employing the patch and reported in [27-28].

Some linearly polarized SIW cavity-backed antennas have also been investigated in [29-32] to attain leaky broadband properties, allay design flexibility, and facilitate easy integration with planner circuits. Nevertheless, SIW offers a small size; however, in some cases, this size could appear more extensive than needed. In this case, An HMSIW is a better solution as it can lessen the size by up to 50% without deteriorating its performance. In addition, two low-profile

antennas are proposed in [33], a joint combination of both HMSIW and patch antenna to form a hybrid antenna.

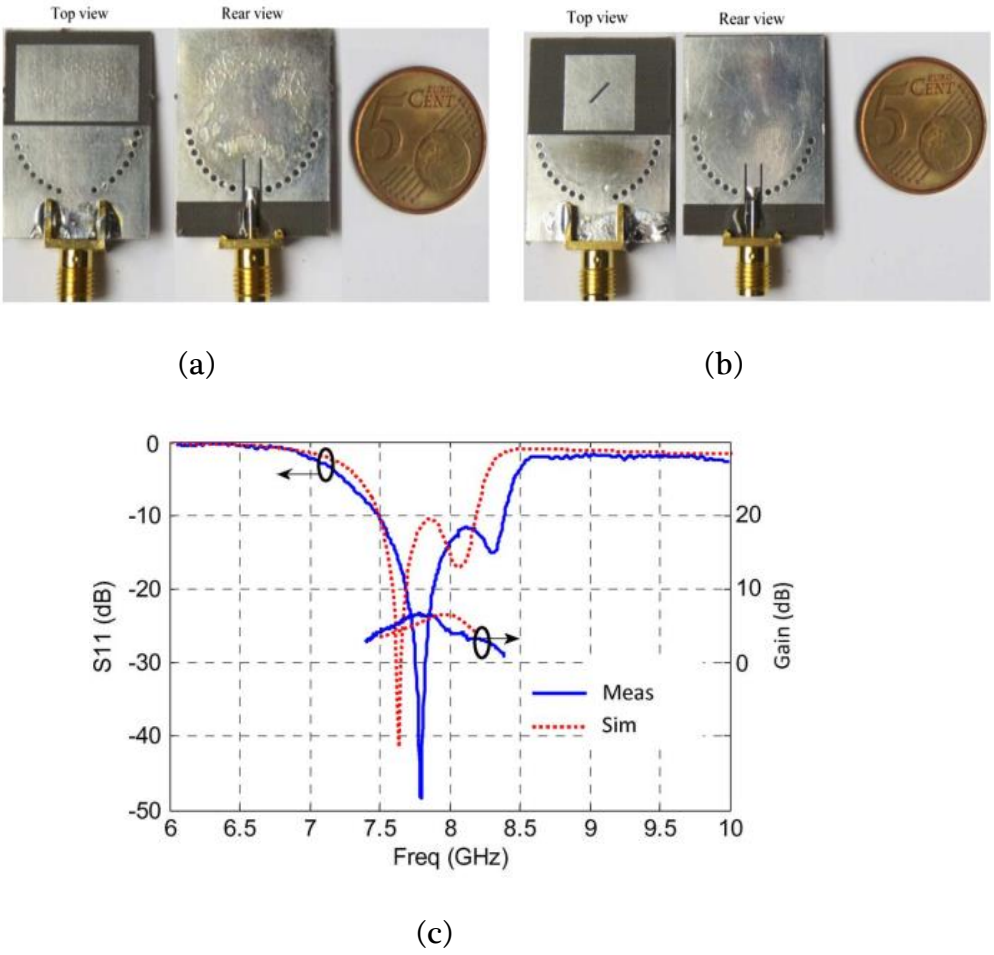

Fig. 2.5. (a) Linearly polarized hybrid antenna and (b) circularly polarized hybrid antenna, (c) return loss of linearly polarized antenna [33].

Chapter 3: Antennas Fundamental Parameters and Substrate Integrated Waveguide

3.1 WHAT IS ANTENNA

An antenna is defined by the IEEE as a "transmitting or receiving system that is designed to radiate or receive electromagnetic waves" [46]. An antenna can be any shape or size. Antennas are a very important component of communication systems. An antenna is a device that converts an electromagnetic signal traveling along a wire into an electromagnetic wave in free space. Antennas have a trait known as reciprocity, which indicates that regardless of whether they are transmitting or receiving, they will maintain the same properties. The majority of antennas are resonant devices that work well across a limited frequency range. Otherwise, reception and transmission would hamper. When a signal is fed into an antenna, the antenna emits a certain type of radiation that is spread in space. A radiation diagram is a graphical representation of the relative distribution of radiated power in space. Wire, aperture, microstrip, reflector, and arrays are examples of typical antenna types. Each antenna arrangement has its own radiation pattern and design factors, as well as advantages and disadvantages.

3.2 ANTENNA PARAMETERS

The fundamental antenna parameters are talked about in this chapter to have a better thought regarding the wireless communication using antenna. Wireless communication is done in the form of waves. Hence, we need to have a look at the properties of waves in communications. This area incorporates with the following parameters-

- ✓ Frequency
- ✓ Wavelength
- ✓ Impedance matching
- ✓ VSWR & reflected power
- ✓ Bandwidth
- ✓ Percentage bandwidth
- ✓ Radiation intensity
- ✓ Antenna aperture
- ✓ Directivity
- ✓ Input Impedance
- ✓ Reflection coefficient
- ✓ Antenna efficiency
- ✓ Gain

3.2.1 Frequency

As per the standard definition, "the rate at which a given wave repeats itself over a given period of time is called as frequency." Mathematically, it is composed as

$$f = \frac{1}{T} \qquad (3.1)$$

Where, *f* can be defined as the frequency of the periodic wave and *T* as the Time period. The unit of frequency is Hertz, represented as Hz.

3.2.2 Wavelength

The wavelength is defined as the difference between two consecutive highest points (tops) or two consecutive lowest points (bottoms). The only thing that separates two quick favorable highs or two prompted adverse peaks of a waveform can be recognized as the duration of that wave. Mathematically, expressed as

$$\lambda = \frac{c}{f} \qquad (3.2)$$

λ is the wavelength, represented in units such as meters of span, *f* can be defined as the frequency of the periodic wave and *c* is the velocity of the light.

3.2.3 Impedance Matching

An impedance matching is the process of designing or matching the antenna's input impedance (Z_L) to the RF circuitry's output impedance (Z_O), which in most

circumstances is 50Ω. The antennas are types of resonant appliances which express superior performance whenever it is matched with respect to load. The necessities for matching of impedance are therefore:

- The energy radiated from the antenna in per unit area will be properly transferred if the impedance of the antenna perfectly matches the impedance of free room.
- The antenna output impedance should be equal with the input impedance of the amplifier receiving antenna system for the receiving unit.
- The input impedance of the transmitter antenna should be equal with the output of the transmitter devices and the impedance of the transmission line impedance (Z) that is represented in Ohms (Ω).

3.2.4 Voltage Standing Wave Ratio (VSWR)

Voltage standing wave ratio (VSWR) is defined as the ratio between transmitted and reflected voltage standing waves in a radio frequency (RF) electrical transmission system. It is a measure of how efficiently RF power is transmitted from the power source, through a transmission line, and into the load. VSWR is a standard voltage wave ratio and is also referred to as Standing Wave Ratio (SWR). VSWR is a parameter that reveals the standing wave condition that is generated due to impedance mismatch between source and the load. The VSWR can be formed as

$$VSWR = \frac{1+|\Gamma|}{1-|\Gamma|} \qquad (3.3)$$

The ratio of reflection is otherwise referred to as S_{11} or loss of exchange. More impedance mismatches lead VSWR to be higher. For effective radiation, the perfect voltage estimate to the standing wave ratio should be 1:1.

where,

Γ = reflection coefficient which is unit less.

3.2.5 Bandwidth

The bandwidth of an antenna refers to the range of frequencies that it can precisely operate on. The bandwidth of an antenna is the number of Hz for which the antenna's SWR is less than 2:1. It's also known as the frequency range between the highest and lowest frequencies at which a signal can be transmitted.

3.2.6 Percentage Bandwidth

"The ratio of complete BW to that bandwidth's center frequency might be referred to as maximum BW," according to the traditional classic idea. The resonant frequency is the frequency within a frequency band where the signal strength is the strongest. It's also called the band's middle frequency (f_c). The higher and lower frequencies are signified f_H and f_L respectively.

- The absolute bandwidth is given by $f_H - f_L$
- Fractional BW or percentage of BW is often used to measure to understand how wider the range is of a particular antenna.

The bandwidth of the percentage is determined to understand how much frequ ency range a section or frame can handle.

$$\text{Percentage BW} = \frac{\text{absolute bandwidth}}{\text{center frequency}} = \frac{f_H - f_L}{f_c} \quad (3.4)$$

The larger the proportion of BW, the wider the BW of an antenna.

3.2.7 Radiation Intensity

Radiation intensity of a given antenna in a given direction can be defined as "energy radiated from an antenna for a solid angle per unit". Radiation intensity is a far-field quantity that can be derived by essentially boosting the radiation density by the split square. It is conveyed as a numerical construct.

$$U = r^2 W_{rad} \quad (3.5)$$

where,

U = radiation intensity (W/unit solid angle)

W_{rad} = radiation density (W/m^2)

r = distance from the antenna

The unit of radiation intensity is Watts/steradian or Watts/radian^2.

3.2.8 Antenna Aperture

Antenna apertures are used in reference to the area of the antenna. It is defined as the measure of the ability of the antenna to effectively receive the power radiated towards it. As the term is associated with the area of the antenna, thus, shows the power capturing characteristics of receiving antennas. The aperture in a general sense signifies a hole or slot present on a surface. Antenna aperture is the term used for the antennas that contain an opening on its surface.

The various types of antenna apertures are as follows:

I. Effective Aperture
II. Scattering Aperture
III. Loss Aperture
IV. Collecting Aperture
V. Physical Aperture

I. **Effective Aperture:** When an electromagnetic wave is transmitted by the transmitting antenna then the receiving antenna present at the other end tries to capture the emitted radiation. We have already discussed in the beginning that antenna aperture is associated with receiving antenna as it talks about the extracting ability of the antenna that is concerned with the reception of the waves. The effective aperture of an antenna is that region of the receiving antenna that effectively collects the electromagnetic energy from the radiated wave out of the overall antenna region. This means greater the extracting region of the antenna more efficient it is. It is defined as the ratio of power received by the antenna to the average power density of the incident wave. Thus, it is given as:

$$Effective\ Aperture = \frac{Power\ Received}{Average\ Power\ Density} \qquad (3.6)$$

$$A_e = \frac{W}{P} \qquad (3.7)$$

Here, W is the received power in watts, P is the average power density in watts/m^2, A_e is the effective area in m^2.

This means that the product of power density of the electromagnetic wave and its aperture is equal to the power received by the antenna.

$$\text{So, } w = A_e * p \qquad (3.8)$$

Hence, an antenna with a larger aperture collects more power than an antenna with a smaller aperture for the same electromagnetic field. Thus, it shows usefulness in calculating the power received by an antenna. Due to reciprocity theorem, the antenna gains for the receiving as well as transmitting modes are same. In a similar way, the effective aperture of the receiving antenna can be used to determine the performance of the transmitting antenna also.

II. **Scattering Loss Apertures:** Previously we have discussed effective aperture that deals with the capturing ability. However, along with this, there exist some other apertures as well. We know that while transmission and reception of signal there exist some considerable losses also. These losses mainly correspond to the radiation and re-radiation resistances and the antenna loss resistance, and this is referred as scattering aperture and loss aperture respectively. This combinedly known as scattering and loss apertures of the antenna. Scattering aperture is denoted as A_s while loss aperture is denoted as A_l.

III. Collecting Aperture: We know that out of the overall power collected by the antenna certain part is associated with the losses due to heat in load and radiation resistance along with antenna loss resistance. These constitute the three apertures of the antenna i.e., effective, scattering and loss. Thus, the summation of the effective (A_e), scattering (A_s) and loss aperture (A_l) as a whole form the collecting aperture of the antenna.

Therefore, is given as:

$$A_c = A_e + A_s + A_l \qquad (3.9)$$

Till now we have discussed the region associated with the antenna that extracts most of the radiating energy from the electromagnetic wave. However, the

physical aperture of the antenna is the actual physical size possessed by the antenna. In antennas like a horn or parabolic reflector, the physical aperture is of great significance because the design of these antennas is quite large. Thus, for large physical size antennas, the physical aperture is a particular and quite important property.

IV. Effective Aperture: The effective aperture of the antenna is designated as the unique property of any type of antenna. It is denoted as A_p and is defined as the physical cross-sectional area of the antenna which is perpendicular to the propagating direction of an electromagnetic wave in order to have a maximum response. It is to be noted here that in the ideal condition of the receiving antenna considering thermal losses to be null, the effective and physical aperture of the antenna is equal. This leads to providing maximum directivity of the antenna.

3.2.9 Directivity

In [47] defines an antenna's directivity as "the ratio of the antenna's radiation intensity in a given direction to the antenna's radiation intensity averaged over all directions". In other words, the directivity of a non-isotropic source is equal to the ratio of its radiation intensity in a given direction, over that of an isotropic source. Antenna Directivity is measured in correspondence to the concentration of the radiated energy by the transmitting antenna specifically in a particular direction. While for the receiving antenna, directivity represents the ability of the antenna to gather most of the radiated energy from a specific direction. Directivity is associated with antenna gain and antenna efficiency. In other words, basically, antenna gain has two components, one is directivity while the other is efficiency.

Thus, the relationship is given as:

$$Antenna\ Directivity = \text{Antenna Gain} * Antenna\ efficiency$$

This implies that the gain of the antenna is the product of directivity and efficiency of the antenna. Directivity is different for different types of antennas.

Generally, for short dipole, its value is 1.76 dB while for large dish antenna it is around 50 dB. It is also called maximum directive gain and is denoted by D. dBi is an abbreviation for "decibels relative to isotropic." While dB is a relative number of the amount of increase or decrease in signal, dBi defines the gain of an antenna system relative to an isotropic radiator.

3.2.10 Input Impedance

The input impedance of an antenna can be portrayed by [47] as "the impedance presented by an antenna at its terminals or the ratio of the voltage to the current at the pair of terminals or the ratio of the appropriate components of the electric to magnetic fields at a point". Hence the impedance of the antenna can be written as:

$$Z_{in} = R_{in} + jX_{in} \tag{3.10}$$

Where,

Z_{in} is the antenna impedance at the terminals

R_{in} is the antenna resistance at the terminals *and*

X_{in} is the antenna reactance at the terminals

The imaginary part, X_{in} of the input impedance represents the power stored in the near field of the antenna. The resistive part, R_{in} of the input impedance consists of two components, the radiation resistance R_r and the loss resistance R_L. The power dissipated in the loss resistance is lost as heat in the antenna itself owing to dielectric or conducting losses, whereas the power associated with radiation resistance R_r is the power actually emitted by the antenna.

3.2.11 Reflection Coefficient

The RC curve (or S_{11}) of an antenna describes how much power are gets reflected to the source due to impedance mismatching between cable and antenna. This value is always negative unlikely return loss (RL). RC and RL have almost similar meaning while analyzing microwave devices but opposite in sign expressed in decibel (dB).

$$RC = -20\log_{10}|\Gamma| \quad (2.11)$$

For perfect matching between the transmitter and the antenna, $\Gamma = 0$ and $RL = \infty$ which means no power would be reflected back, whereas a $\Gamma = 1$ has a $RC = 0$ dB, which implies that all incident power is reflected. For practical applications, a VSWR of 2 is acceptable, since this corresponds to an RC of -9.54dB.

3.2.12 Antenna Efficiency

The antenna efficiency is a parameter which takes into account the number of losses at the terminals of the antenna and within the structure of the antenna. These losses are given by [47] as:

- Reflections because of mismatch between the transmitter and the antenna
- I^2R losses (conduction and dielectric)

Hence the total antenna efficiency can be written as:

$$e_t = e_r + e_c + e_d \quad (2.12)$$

where,

e_t = total antenna efficiency

$e_r = (1 - |\Gamma|^2)$ = reflection (mismatch) efficiency

e_c = conduction efficiency

e_d = dielectric efficiency

Since e_c and e_d are difficult to separate, they are lumped together to form the e_{cd} efficiency which is given as:

$$e_{cd} = e_c e_d = R_r/(R_r + R_L) \quad (2.13)$$

e_{cd} is called the antenna radiation efficiency and is defined as the ratio of the power delivered to the radiation resistance (R_r) to the power delivered to R_r and R_L (load resistance).

3.2.13 Gain

Antenna gain is a parameter that is proportional to the directivity of the antenna. We already know that an antenna's directivity relates to how much energy it concentrates in one direction vs others. As a result, the antenna gain would be equal to directivity, and the antenna would be an isotropic radiator if it were 100 percent effective. The gain is always related to the main lobe and is specified in the direction of maximum radiation unless indicated. It is given as:

$$G(\theta,\varphi) = e_{cd}\, D(\theta,\varphi) \text{ (dBi)} \qquad (3.14)$$

3.3 ANTENNA FIELD REGIONS

The antenna space made up of three fields (a) near-field linear, (b) near-field (Fresnel) and (c) far-field (Fraunhofer) as shown in Fig. 3.1. These regions are distributed to separate the arrangement of the segment in each locale.

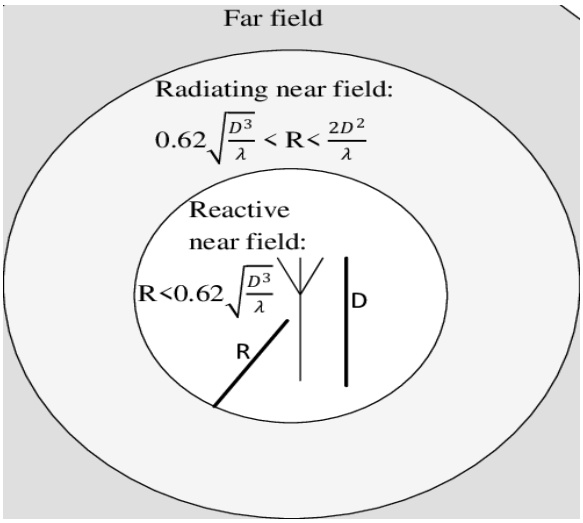

Fig. 3.1. The different field region of the antenna [48]

Albeit no surprising alterations are seen as the limits are passed in the area arrangement, there are distinctive differences among them. The boundaries that isolate these sites are not outstanding, although distinct requirements have been established and are used frequently to differentiate the sites.

When the radiation intensity is measured closer to the antenna, it compares to what is measured further away. Despite the fact that the area is far from the

antenna, it is regarded practical because the radiation intensity is still considerable. The usual amplitude patterns in several places of field region are depicted in Fig. 3.2.

3.3.1 Reactive Near-Field Region

The reactive near-field region is the portion of the near-field region surrounding the antenna where the reactive field dominates. For most antennas, the external limit of this locale is usually assumed to exist at a separation between $R< 0.62\sqrt{D^3/\lambda}$ and the antenna surface, where λ is the wavelength and D is the largest component of the antenna.

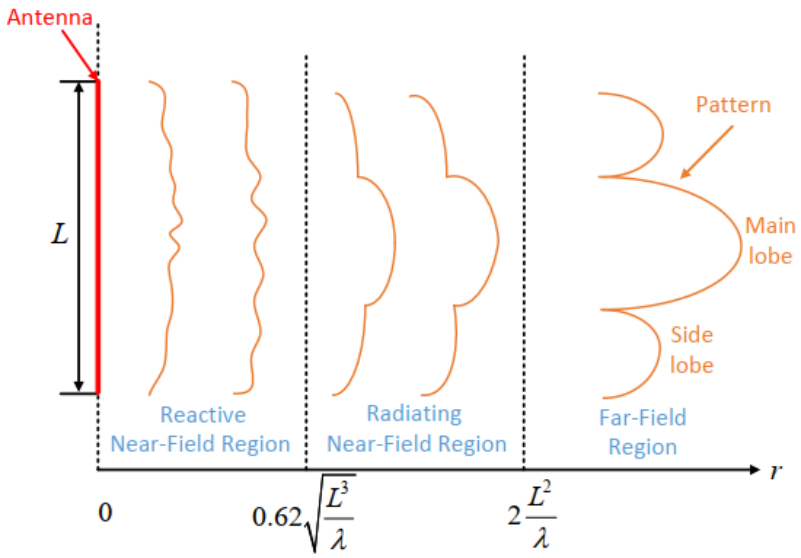

Fig. 3.2. Antenna amplitude pattern shape from reactive near field toward the far field [49]

3.3.2 Radiating Near-Field (Fresnel) Region

Emanating close field (Fresnel) area is characterized as that area of the receiving wire field between the flexible close field district and the far-field locale where radiation conditions win and where the dashing field stream needs isolation from the reception apparatus. The inner boundary is taken to be the distance $R \geq 0.62\sqrt{D^3/\lambda}$ and the outer boundary the distance $R < 2D^2/\lambda$.

3.3.3 Far-field (Fraunhofer) region

The far field is the part of the field where it behaves like 'normal' electromagnetic radiation. The electric or magnetic fields with electric dipole properties dominate this region. If the antenna having a maximum dimension D, it is commonly assumed that the far-field region exists at distances greater than $2D^2/\lambda$ from the antenna, λ being the wavelength.

3.3.4 Beam Width

Beam width is also considered as another important factor in the radiation pattern of an antenna. The main lobe of the radiation pattern of an antenna is the main beam of the antenna where maximum and constant energy radiated by the antenna flows.

Beam width is the hypothetical aperture angle from where most of the power is radiated. The two main considerations of this beam width are Half Power Beam Width (HPBW) and First Null Beam Width (FNBW) shown in Fig. 3.3 and 3.3 respectively.

3.3.4.1 Half-Power Beam Width

According to the standard definition, "The angular separation, in which the magnitude of the radiation pattern decreases by 50% (or -3dB) from the peak of the main beam, is the Half Power Beam Width (HPBW)."

In other words, the beam width is the area where the majority of the power, or peak power, is emitted. When a line is drawn between radiation pattern's origin and the half power points on the major lobe, on both the sides, the angle between those two vectors is termed as HPBW, half power beam width. This can be well understood with the help of the Fig. 3.3.

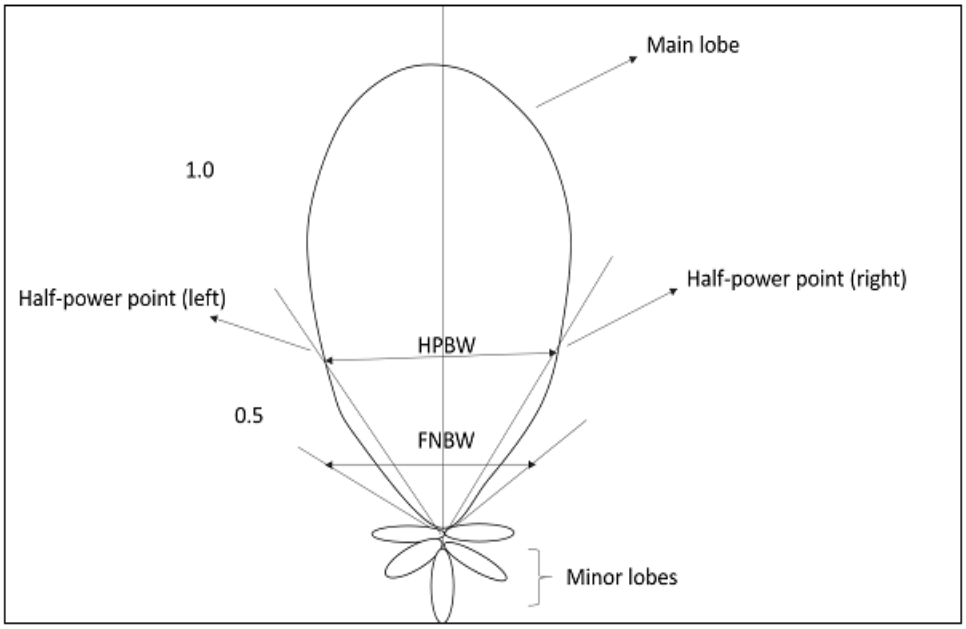

Fig. 3.3. HPBW and FNBW [50]

HPBW can be mathematically expressed like,

$$\text{Half-power beamwidth} = 70\lambda/D \tag{2.15}$$

where,

λ is the wavelength *(λ = 0.3/frequency)* and

D is diameter and then unit will be radians or degree.

3.3.4.2 First-Null Beam Width

As per the definition, "The angular span between the first pattern nulls adjacent to the main lobe, is called as the First Null Beam Width (FNBW)." Simply, FNBW is the angular spacing between the null points of the radiation pattern on its major lobe, measured away from the main beam. When a tangent is drawn on both sides of the radiation pattern, tangential to the primary beam, starting from the origin. The angle between those two tangents, known as FNBW is shown clearly in Fig. 3.4.

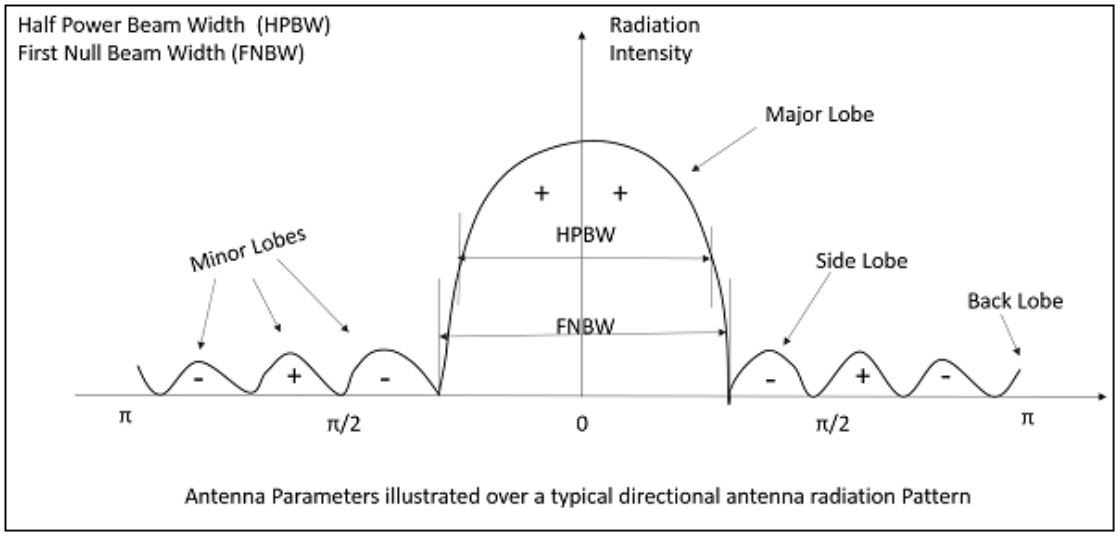

Fig. 3.4. The HPBW and FNBW is marked in a radiation pattern along with minor and major lobes [50]

The mathematical expression of FNBW is,

$$\text{FNBW} = 2\ \text{HPBW} \tag{3.16}$$

$$\text{FNBW}\ 2(70\lambda/D) = 140\lambda/D \tag{3.17}$$

where,

λ is the wavelength *($\lambda = 0.3/frequency$)* and

D is diameter and then unit will be radians or degree.

3.4 MICROSTRIP PATCH ANTENNA (MPA)

Deschamps [51] was the first to propose the concept of a microstrip antenna. The first antenna was designed by Howel and Munson in the 1970s when suitable substrates with low loss tangent and appealing thermal and mechanical qualities became accessible, and improved theoretical models became available. Microstrip antennas have evolved since then to become one of the most appealing antenna solutions in a variety of current microwave communication systems.

A microstrip antenna consists of a pair of parallel conducting layers separated by a dielectric medium, referred to as the dielectric substrate, as shown in Fig. 3.5. The upper conducting layer or patch mounted on the dielectric substrate is

the source of radiation in this setup, where electromagnetic energy fringes off the patch's edges and into the substrate. On the other side of the substrate, the lower conducting layer serves as a perfect reflecting ground plane, bouncing energy back through the substrate and into free space.

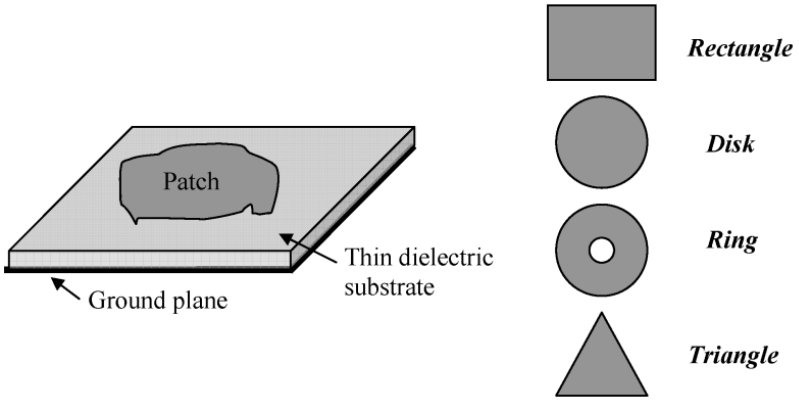

Fig. 3.5. The microstrip antenna with its basic structure [51]

Fig. 3.5 depicts the microstrip patch antenna's basic structure. It is comprised of a metallized area maintained above a ground plane by a thin dielectric substrate and supplied against the ground at a suitable point. In theory, the patch shape can be anything; in practice, the rectangle, circle, equilateral triangle, and annular ring are frequent shapes.

3.4.1 Advantages and Disadvantages of Microstrip Patch Antennas

3.4.1.1 Advantages

The advantages of microstrip patch antennas are:

- Planar, which can also be made conformal to a shaped surface.
- Low profile and minimum radar cross-section
- Rugged and can be manufactured by printed circuit technology.
- Integrable with circuit elements
- Can be made suitable for dual polarization operations.

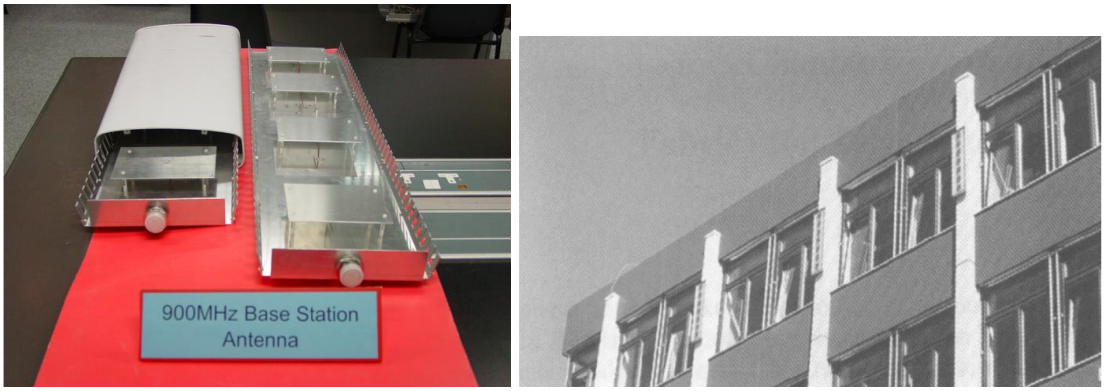

(a) (b)

Fig. 3.6. (a) A base station antenna array consisting of patches and (b) patch antenna arrays mounted on the walls of a building. [52]

Because of the advantages listed above, the microstrip patch antenna has also become the favorite of antenna designers for commercial mobile and wireless communication systems. Fig. 3.6(a) shows a base station antenna array consisting of patches. Fig. 3.6 (b) shows patch antenna arrays mounted on the walls of a building for satellite television reception.

3.4.1.2 Disadvantages

There are several disadvantages associated with microstrip patch antennas.

- The microstrip antenna has a limited impedance bandwidth in its most basic form, often less than 5%. Various bandwidth-widening approaches, on the other hand, have been developed. It has been possible to gain bandwidth of up to 50%.
- The microstrip antenna can manage relatively low RF power due to the tiny spacing between the radiating patch and its ground plane.
- Because a single patch element is only roughly one-half wavelength, microstrip arrays have a higher ohmic loss than arrays of other types of antennas with similar aperture size. The dielectric substrate and metal conductor of the microstrip line feed network and power dividing circuit experience the largest ohmic loss.

3.4.2 Material Consideration

Normally, the metallic patch is made of thin copper foil. The radiating patch elements are mechanically supported by the substrate material. It also keeps the patch and its ground plane at the proper distance. For the basic geometry, the substrate thickness is in the range of 0.01 to 0.05 free-space wavelength.

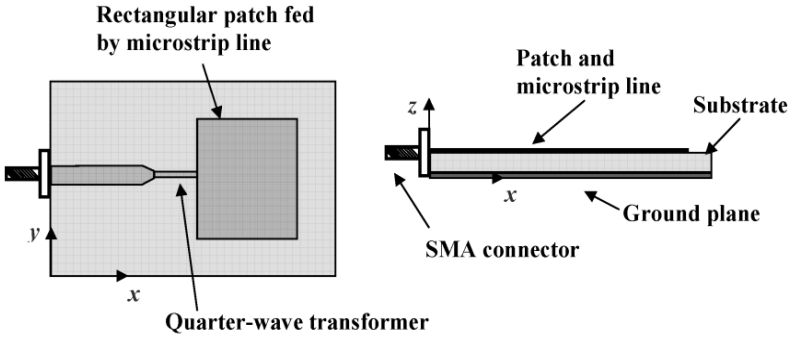

(a) (b)

Fig. 3.7. The geometry of a direct microstrip feed microstrip patch antenna (a) top view and (b) side view [53]

The dielectric constant ranges from 1 to 10 and can be separated into three categories.

- Those having a relative dielectric constant (relative permittivity) in the range of 1.0 to 2.0. This type of material can be air, polystyrene foam, or dielectric honeycomb.

- Those having a relative dielectric constant in the range of 2.0 to 4.0. This type of material consists mostly of Fiberglass reinforced Teflon.

- Those with a relative dielectric constant between 4.0 and 10.0. This type of material can be ceramic, quartz, or alumina.

The most used material is Teflon-based with a relative permittivity between two and three. This material is also called PTFE (Polytetrafluoroethylene). It has a structure that is identical to that of fiberglass, which is utilized for digital circuit boards, but with a much smaller loss tangent. As seen in the samples below, cost,

power loss, and performance are all factors to consider when selecting a substrate material. At the L-band frequency, for example, a single patch or a few-element array may be manufactured on a low-cost fiberglass material, whereas a 20-element array at 30 GHz may require a higher-cost, but lower-loss Teflon-based material (loss tangent less than 0.005). A dielectric honeycomb or foam panel can be used as a substrate for many array elements at lower microwave frequencies (below 15 GHz) to reduce loss, antenna mass, and material cost while increasing bandwidth performance. Materials with a relative dielectric constant greater than 10 exist. For a larger dielectric constant, the patch size is lower. Higher dielectric constants, on the other hand, limit bandwidth and radiation efficiency.

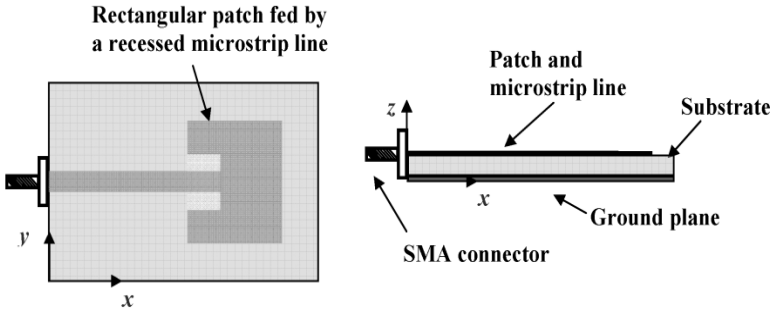

(a) (b)

Fig. 3.8. The geometry of a recessed microstrip line feed microstrip patch antenna (a) top view and (b) side view. [53]

3.5 THE SINGLE ELEMENT FEEDING TECHNIQUE

3.5.1 The microstrip line feed

The patch is fed via a microstrip line that is on the same plane as the patch in microstrip feed. Both the feeding and the patch are combined in this example. Modeling, matching, and fabricating microstrip feed is simple. It's also an excellent choice for antenna-array feeding networks. Microstrip feed, on the other hand, has the disadvantage of having a small bandwidth and introducing coupling between the feeding line and the patch, which causes spurious radiation

[34], as well as requiring matching between the microstrip patch and the 50Ω feeding line. Microstrip feed is divided into three categories:

3.5.1.1 Direct feed: The feeding point is on one of the patch's edges. Direct feed requires a matching network between the feed line and the patch, as shown in Fig. 3.7. (Such as quarter wavelength transformer). The impedance variations between the patch and the 50Ω feed line are compensated by the quarter wavelength transformer. [34] provides formulas for calculating the quarter wavelength transformer.

3.5.1.2 Inset feed: where the feeding point is inside the patch. The location of the feed is the same as that will be used for coaxial feed. The 50 Ω feed line is surrounded with an air gap till the feeding point as shown in Fig. 3.8. The inset microstrip feeding technique is more suitable for arrays feeding networks [34].

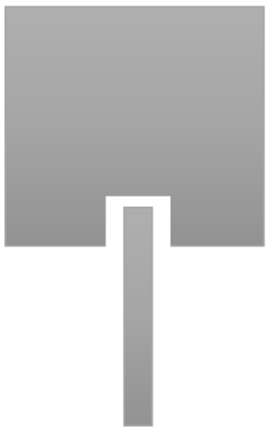

Fig. 3.9. The gap coupled patch antenna.

3.5.1.3 Gap-coupled: The feeding line does not contact the patch; there is an air gap between the 50 Ω line and the patch as shown in Fig. 3.9. The antenna is fed by coupling between the 50 Ω feed line and the patch.

3.5.2 Coaxial probe feed

It's one of the most essential microwave energy delivery techniques for an antenna. The coaxial cable's outer conductor is soldered to the metal patch, while the inner conductor is connected to the ground plane [40]. Coaxial feeding is simple to design in Fig. 3.10, construct, and match, and it creates very little unwanted radiation [53]. Coaxial feeding, on the other hand, has the drawback of requiring extremely precise soldering. Due to the large number of solder joints required, using coaxial feeding with an array is difficult. A longer probe is necessary when a thick substrate is used, which increases the surface power and feed inductance [53].

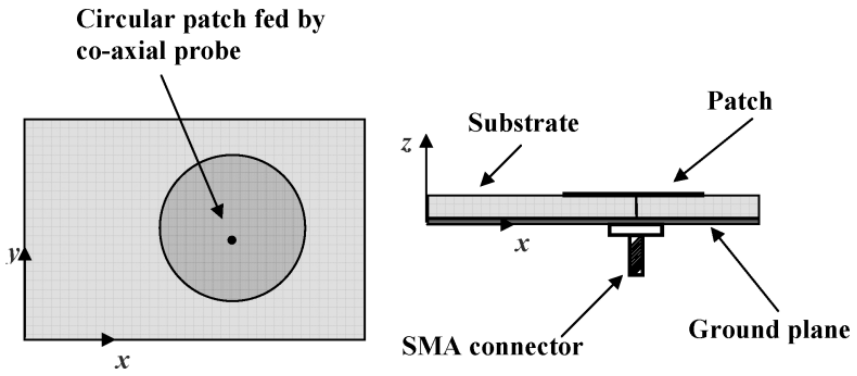

(a) (b)

Fig. 3.10. The geometry of coaxial probe feed microstrip patch antenna (a) top view and (b) side view. [53]

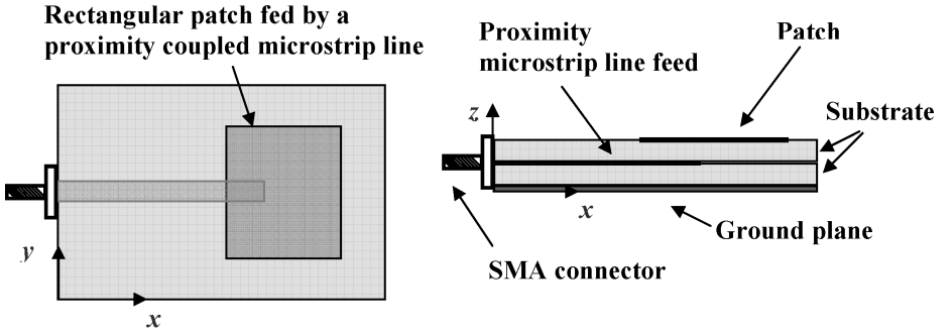

(a) (b)

Fig. 3.11. The geometry of a proximity coupled microstrip feed microstrip patch antenna (a) top view and (b) side view. [53]

3.5.3 Proximity (Electromagnetically) coupled microstrip feed

Proximity connected feeding is made up of two dielectric substrate layers. The microstrip patch antenna is on top of the upper substrate, while the microstrip feeding line is on top of the bottom substrate, as shown in Fig. 3.11.

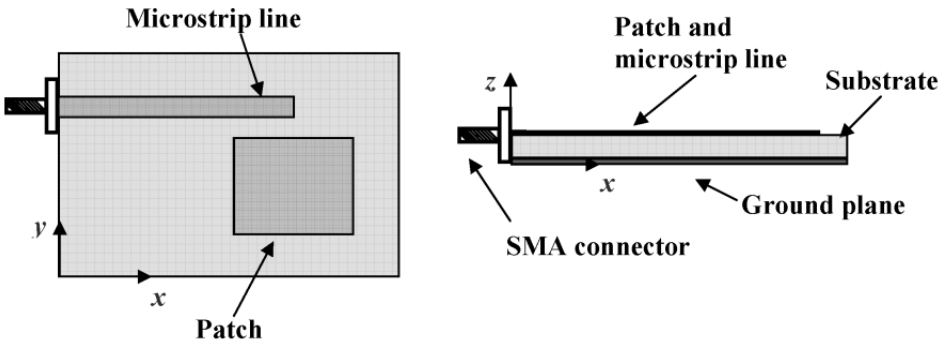

Fig. 3.12. The geometry of a patch antenna fed by an adjacent microstrip line (a) top view and (b) side view. [53]

It's a non-contact feed that feeds the microstrip line via electromagnetic coupling between the patch and the microstrip line. The properties of the two substrates can be chosen differently to optimize antenna performance [53]. While improving bandwidth, the proximity coupled feeding method avoids undesired radiation. However, precise alignment between the two layers is essential in multilayer fabrication.

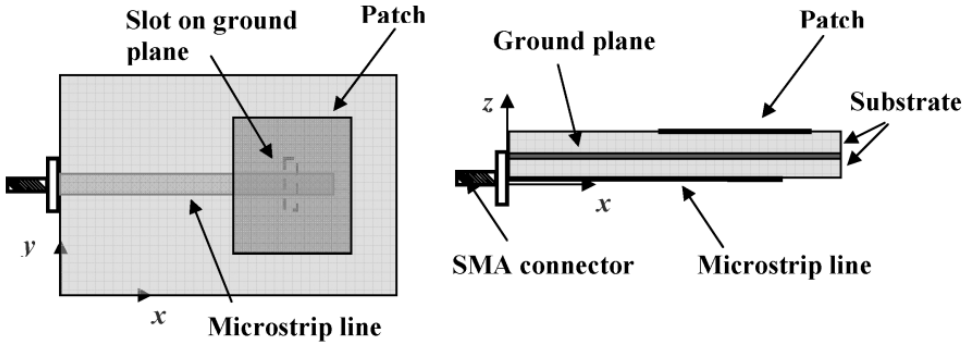

Fig. 3.13. The geometry of an aperture coupled feed microstrip patch antenna (a) top view, (b) side view. [53]

An open-ended microstrip line can also be placed in parallel and very close to the edge of a patch, to achieve excitation through fringe-field coupling, as shown in Fig. 3.12. Both methods avoid any soldering connection, which in some cases, could achieve better mechanical reliability.

3.5.4 Aperture-coupled microstrip feed

Two substrate layers are used in aperture coupled feeding, with a common ground plane in between them. As illustrated in Figs. 3.13 and 3.14, the microstrip patch antenna is on top of the higher substrate and the microstrip feeding line are on the bottom of the lower substrate, with a slot cut in the ground plane. The slot, which can be any size or shape, is utilized to boost the antenna's performance. It's a contact-free feed. The feeding is done through electromagnetic coupling between the patch and the microstrip line through the slot in the ground plane. The two substrates' parameters can be chosen different than each other to enhance antenna performance [53].

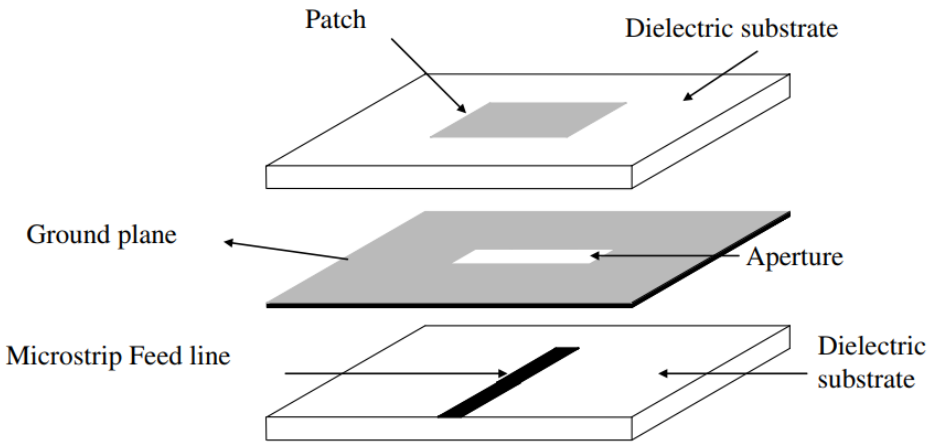

Fig. 3.14. The pictorial view of an aperture coupled feed microstrip patch antenna. [53]

3.6 TYPES OF MICROSTRIP ANTENNA

3.6.1 Planner Inverted-F Antenna

An inverted-F antenna can be considered, a type of antenna used in wireless communication, mainly at UHF and microwave frequencies. It consists of a monopole antenna running parallel to a ground plane and grounded at one

end. The antenna is fed from an intermediate point a distance from the grounded end. The design has two advantages over a simple monopole: the antenna is shorter and more compact, allowing it to be contained within the case of the mobile device, and it can be impedance matched to the feed circuit by the designer, allowing it to radiate power efficiently, without the need for extraneous matching components.

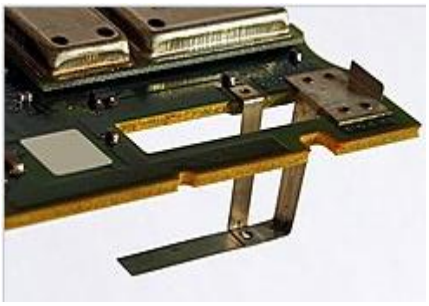

Fig. 3.15. A PIFA antenna. [54]

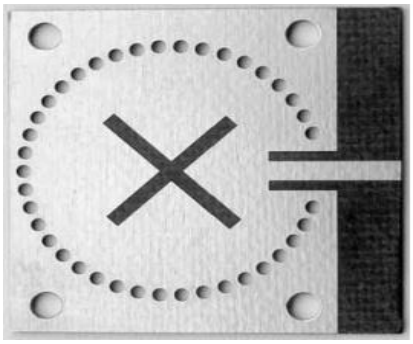

Fig. 3.16. Photo of fabricated SIW antenna. [55]

The inverted-F antenna was first conceived in the 1950s as a bent-wire antenna. However, its most widespread use is as a planar inverted-F antenna (PIFA) in mobile wireless devices for its space saving properties. PIFAs can be printed using the microstrip format, shown in Fig. 3.15, a widely used technology that allows printed RF components to be manufactured as part of the same printed circuit board used to mount other components.

3.6.2 Substrate Integrated Waveguide (SIW) Antenna

A SIW (also known as post-wall waveguide or laminated waveguide) is a synthetic rectangular electromagnetic waveguide formed in a dielectric substrate by densely arraying metallized posts or via holes that connect the upper and lower metal plates of the substrate. The waveguide can be easily fabricated with low-cost mass-production using through-hole techniques, where the post walls consists of via fences. SIW is known to have similar guided wave and mode characteristics to conventional rectangular waveguide with equivalent guide wavelength.

The rectangular waveguide topology can overcome these issues, as it offers an excellent immunity against radiation losses and presents low insertion losses. But in their classical form, rectangular waveguide is not compatible with the miniaturization required by modern applications. However, by cutting slot or employing an opening in the structure of the SIW, shown in Fig. 3.16, this can be converted into a radiator, SIW antenna. Many SIW antenna have been proposed in recent year as they allow to have high gain. Low sidelobe levels and elevated boresight gain.

3.6.3 Vivaldi Antenna

The feeding line excites an open space via a microstrip line or coaxial cable, and may be terminated with a sector-shaped area or a direct coaxial connection. From the open space area, the energy reaches an exponentially tapered pattern via a symmetrical slot line.

Fig. 3.17. The photo is of fabricated Vivaldi antenna. [56]

Vivaldi antennas, is shown Fig. 3.17, can be made for linear polarized waves or using two devices arranged in orthogonal direction for transmitting / receiving both polarization orientations. If fed with 90 degree phase-shifted electromagnetic signals, orthogonal devices can transmit/receive circular oriented electromagnetic waves. Vivaldi antennas are useful for any frequency, as all antennas are scalable in size for use at any frequency. Printed circuit technology makes this type of antenna cost effective at microwave frequencies

exceeding 1 GHz. Advantages of Vivaldi antennas are their broadband characteristics (suitable for ultra-wideband signals).

3.7 POLARIZATION

Polarization is the feature that specifies a wave's electric field rotation at a fixed place as a function of time as it travels across space. It's a characteristic that stays the same across the antenna's main beam but varies in the smaller loops. Because the electric and magnetic field vectors are always connected by Maxwell's equation, it is sufficient to define the polarization of one of them, which is usually the electric field. IEEE Standard should be used to determine polarization in its transmitting mode. The polarization plane is always perpendicular to the propagation plane and contains the electric and magnetic field vectors. The wave polarization is described by the contour created by the tip of the electric field vector. An ellipse, circle, or line is the shape of this contour. Unless otherwise noted, the polarization is assumed to be in the direction of maximal gain.

Co- and cross-polarizations (XPL) are the two types of polarization for EM field. The polarization radiated/received by the antenna is co-polarization, whereas cross-polarization is perpendicular to it. In wave propagation between the transmitting and receiving antennas, polarization is critical. The receiving antenna must have the same polarization and sensibility as the outgoing wave to extract the signal. When the receiving antenna has the same direction, axial ratio, spatial orientation, and sense of polarization as the incident wave, maximum power transmission occurs; otherwise, polarization mismatch occurs. If there is a polarization mismatch, it will result in further losses.

3.7.1 Types of Polarization

There are three types of polarization: linear polarization, elliptical polarization, and circular polarization.

3.7.1.1 Linear Polarization

An antenna has linear polarization if the field vector (electric or magnetic) for the transmitted wave of the antenna only has one component or two orthogonal linear component that are in same phase or 180° (or multiples of 180°) out of phase [34]. Fig. 3.18 shows that the electric field propagates in one plane and so the magnetic field propagates in the plane orthogonal to that. Fig. 3.19 shows that the linear polarized wave can propagate in two different planes. When it propagates in the horizontal plane, it is horizontal linear polarization and in the vertical plane it is vertical linear polarization.

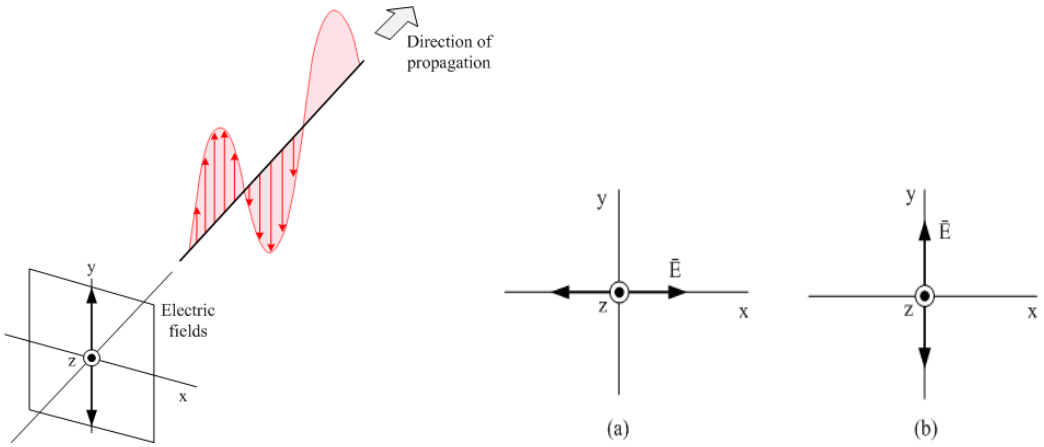

Fig. 3.18. Linear polarization [57] Fig. 3.19. Linear polarization (a) Horizontal (b) Vertical.

3.7.1.2 Elliptical polarization

If the field vector (electric or magnetic) for the antenna's transmitted wave has two orthogonal linear components of equal or different magnitude, the antenna has elliptical polarization. When the magnitudes of these components differ, the time-phase difference between them cannot be 0° or multiples of 180°, or linear polarization would result. Because circular polarization occurs when the two components have the same magnitude, the time-phase difference between them

must not be odd multiples of 90°. The propagation of the elliptically polarized wave is depicted in Fig. 3.20. At the same time, the electric field propagates in two planes with distinct amplitudes.

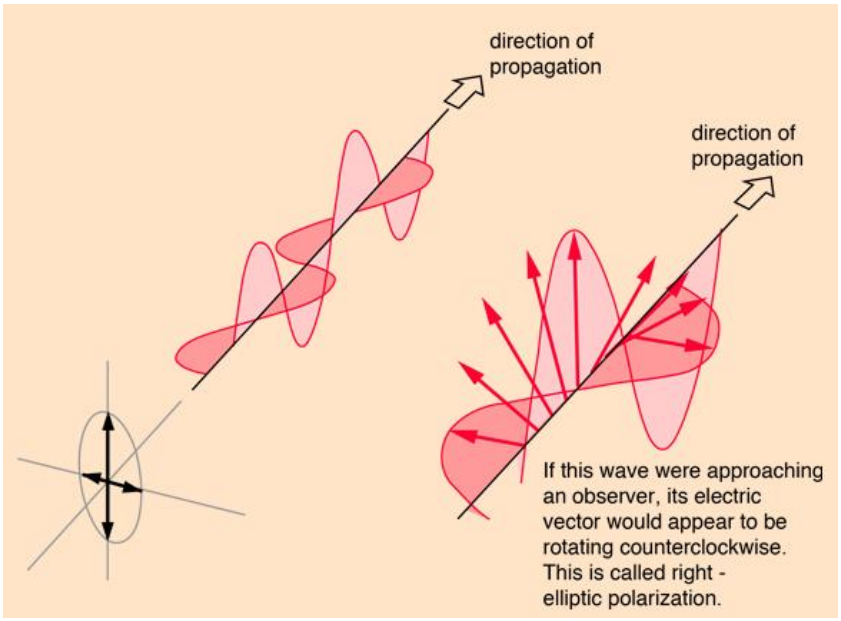

Fig. 3.20. The elliptical polarization [57]

3.7.1.3 Circular polarization

If the field vector (electric or magnetic) for the antenna's transmitted wave contains two orthogonal linear components with the same magnitude and the time-phase difference between them is odd multiples of 90°, the antenna has circular polarization (CP). Circular polarization can be divided into two categories. Right-hand circular polarized (RHCP) if the field rotates clockwise, and left-hand circular polarized (LHCP) if the field rotates counterclockwise [58].

The circular polarized wave propagates as shown in Fig. 3.21. The electric field propagates in two planes with identical amplitude at the same time. The electric field rotates clockwise (LHCP) and counterclockwise (LHCP) as shown in Fig. 3.22 (RHCP).

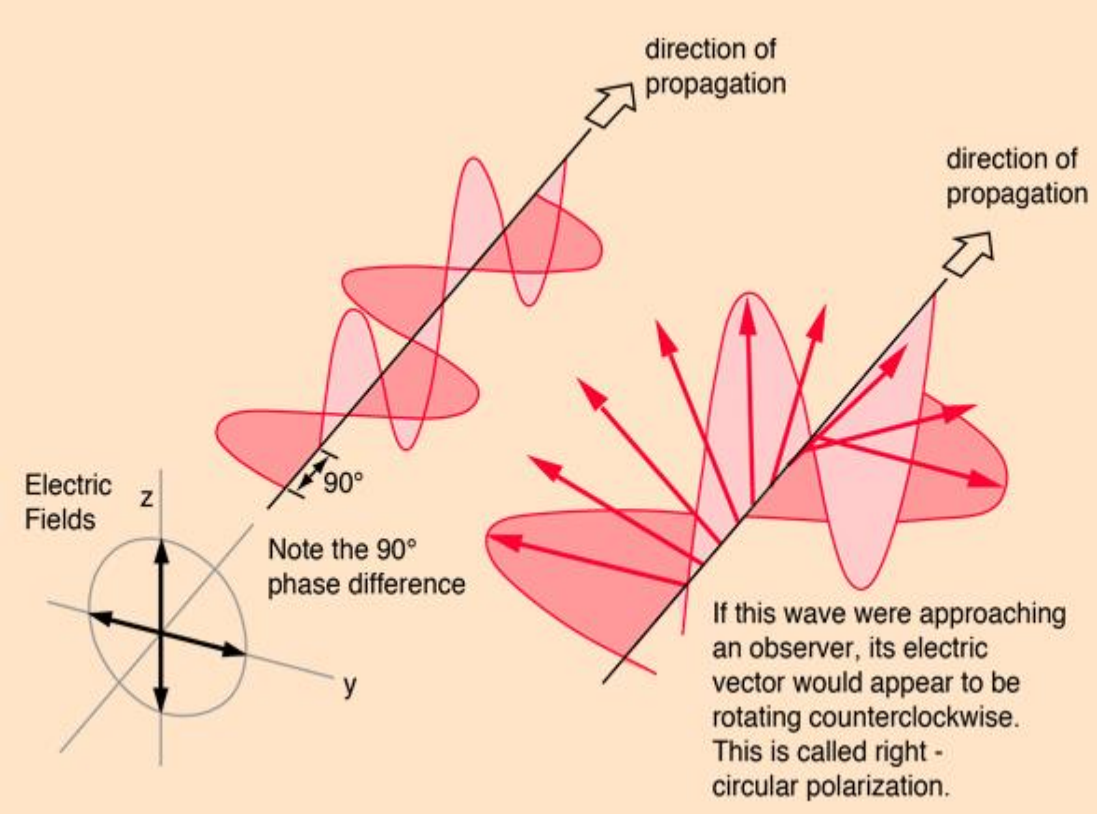

Fig. 3.21. The circular polarization [57]

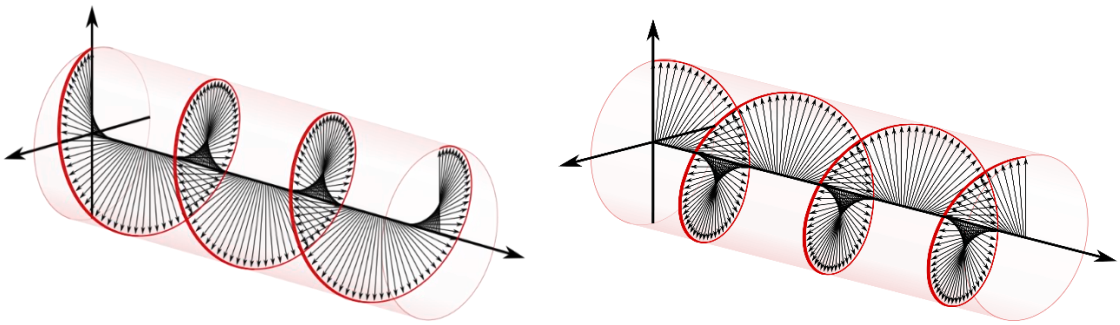

Fig. 3.22. The circular polarization (a) LHCP (b) RHCP. [59]

3.7.2 *Axial Ratio*

E-field and H-field are main ingredients of EM wave, and the vibration direction of E-field normally determines the axis of polarization. There are three types of polarization such as LP, CP, and elliptical polarization (EP). In the case of LP E-field vibrates only one axis but for CP and EP it vibrates in two axes.AR normally indicates these ratios of orthogonal components of E-field in EP. If AR<3 dB it assumes that antenna has CP as practically antenna cannot attain

0dB.An ideal axial ratio value for CP is 1 or (0 dB) because in that case two components of E-field possess equal magnitude and remain separate by 90° out of phase. In simulated cases of an antenna shows a defective polarization and tailed out to EP in lieu of CP. Also, worth noted that in authentic LP, its axial ratio amplified to infinite due to one E-field component.

In a general case, the electric field of a propagating electromagnetic wave traces out an ellipse in the plane normal to the direction of propagation. According to the notation used in Fig. 3.23, the polarization ellipse is characterized by its maximum and minimum field values (OA and OB), the sense of rotation, and the tilt angle (τ). The axial ratio (AR) is defined as

$$AR = \frac{major\ axis}{minor\ axis} = \frac{\mathrm{OA}}{OB} = \frac{|\mathrm{Emax}|}{|\mathrm{Emin}|} \qquad (2.23)$$

According to the previous definition, pure circular polarization corresponds to $|AR| = 1$, and in the case of linear polarization the axial ratio goes to infinite. These are the two extreme conditions, so any other case corresponds to elliptical polarization with certain axial ratio $1 \leq |AR| \leq \infty$.

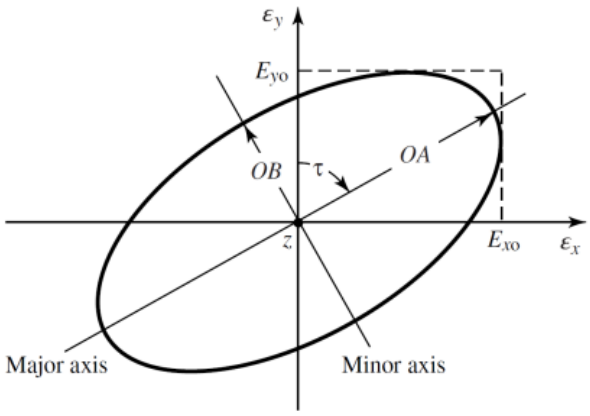

Fig. 3.23. Axial ratio: An electric field created by two electric field components. [60]

3.8 THE SUBSTRATE INTEGRATED WAVEGUIDE (SIW) TECHNOLOGY

In recent years, interest in utilizing millimeter-waves (mm-waves) has significantly increased. Mm-waves occupy the frequency spectrum from 30-300 GHz. The reason behind the increased interest in using mm-waves is the inherent advantages these waves offer such as broadband and high-resolution techniques. A variety of applications using mm waves have been recently proposed including wireless networks, automotive radars, imaging sensors and biomedical devices [61]. At frequencies lower than mm-waves, system components are typically fabricated in planar technology (microstrip or coplanar waveguides). However, at frequencies higher than 30 GHz microstrip and coplanar waveguides suffer from transmission losses and radiation while cylindrical waveguides, though they have low loss, are expensive and complex to integrate with planar circuit. Therefore, for successful development of mm-wave systems there is a need for technology that enables the implementation of different system components with high performance and low cost.

One such technology that has been recently explored by researchers is SIW. SIW is a new form of transmission line. Fig. 3.24 shows the geometry of an SIW structure. SIW technology enables the implementation of classical non-planar rectangular waveguide (RWG) in planar form. Fig. 3.25 shows the geometry of an RWG. The vertical side walls of the RWG are replaced by the two rows of metal vias in an SIW. Moreover, SIW technology conforms with existing planar fabrication techniques such as PCB.

Furthermore, SIW structures preserve most of the advantages of conventional metallic waveguides including high quality-factor and high power-handling capability. However, the most significant advantage of SIW technology is the possibility to integrate different system components on the same substrate, including passive and active elements and even antennas.

3.8. 1 Rectangular Waveguide Theory

RWGs are one of the earliest forms of transmission line and they are used to transport microwave signals. As the name suggests and as shown in Fig. 3.25, RWGs have rectangular cross-section. Also, RWGs can be hollow (filled with air) or filled with a material of electric permittivity ε and magnetic permeability μ. There are various RWG components such as couplers, detectors, isolators, attenuators, and slotted lines that are commercially available.

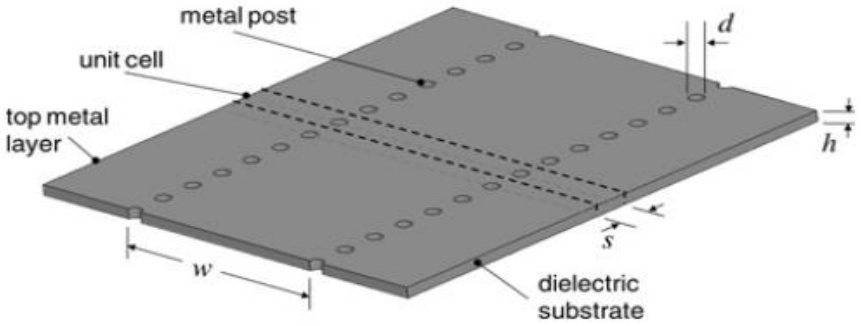

Fig. 3.24. Geometry of SIW (w: width of SIW, d: diameter of metal vias, s: longitudinal via spacing, h: substrate thickness) [61]

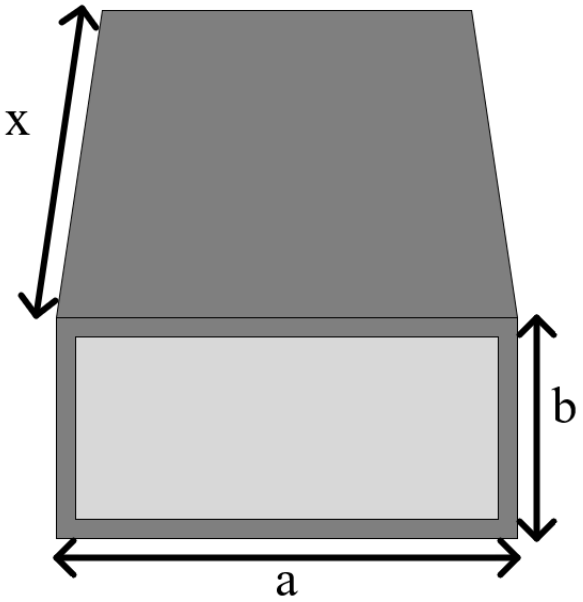

Fig. 3.25 Geometry of RWG (a: width of RWG, b: height of RWG, x: length of RWG).

and operating from 1-220 GHz. One disadvantage of RWGs is that they are bulky, thus, they cannot be easily integrated with miniaturized circuits and systems. In this case, planar transmission lines are utilized such as microstrip and stripline. There is also the concept of propagating modes in RWGs which will be described briefly here along with key theoretical equations. Based on a Cartesian coordinate system, there are two types of modes that can propagate in RWGs: namely, transverse electric (TE) and transverse magnetic (TM) modes. TE modes are those having no electric field components in the modes' direction of propagation. Only TE modes will be discussed briefly here along with relevant theoretical equations since they are the only TE modes that can propagate in SIW structures. For TM modes, structure needs continuous current alongside its wall, however vias are discrete resulting in no continuous current. For each TE mode a propagation constant β is defined as follows [62]:

$$\beta = \sqrt{k^2 - k_c^2} = \sqrt{k^2 - \left(\frac{m\pi}{a}\right)^2 - \left(\frac{n\pi}{b}\right)^2} \qquad (3.16)$$

where k is the wavenumber of the material filling the RWG ($k = \omega\sqrt{\mu\varrho} = 2\pi f\sqrt{\mu\varrho}$), k_c is the cutoff wavenumber, a and b are the width and height of RWG respectively as shown previously in Fig. 3.25. β of a TE mode is an important quantity in which having a real value corresponds to a propagating mode. Based on (3.16), β can be real only when

$$k > k_c = \sqrt{\left(\frac{m\pi}{a}\right)^2 + \left(\frac{n\pi}{b}\right)^2} \qquad (3.17)$$

where,

$$K_c = \omega_c\sqrt{\mu\varepsilon} = 2\pi f_c\sqrt{\mu\varepsilon} \qquad (3.18)$$

As it can be seen from (3.18), k_c is a function of frequency (f_c) and the filling material. Therefore, β is a function of frequency as well as the geometry of the

guide. Also, based on (3.18) and (3.17) each TE mode has a cutoff frequency given by-

$$f_c = \frac{k_c}{2\pi\sqrt{\mu\varepsilon}} = \frac{1}{2\pi\sqrt{\mu\varepsilon}}\sqrt{\left(\frac{m\pi}{a}\right)^2 + \left(\frac{n\pi}{b}\right)^2} \qquad (3.19)$$

The mode with the lowest cutoff frequency is called the fundamental/dominant mode. Assuming a > b, the lowest fc occurs for TE_{10} (m = 1, n = 0) mode which is reduced from (3.19) to be

$$f_{c_{TE10}} = \frac{1}{2a\sqrt{\mu\varepsilon}} \qquad (3.20)$$

For further detail about RWG theory, [85] is an excellent resource.

3.9 SIW STRUCTURES

3.9.1 Operation Principles of SIW structures

As mentioned earlier, SIW structures in Fig. 3.23 exhibit propagation characteristics like RWGs, provided that the metallic vias are closely spaced and leakage between the via gaps can be neglected [33]. Specifically, SIW modes are like a subset of guided modes in a RWG, namely TE_{m0} modes with m = 1, 2, ... For example, the fundamental mode of an SIW is like the fundamental TE_{10} mode of a RWG, with vertical electric current density on the side walls. Since the vertical metal walls in a RWG are replaced by via fences for SIW structures, propagating modes of SIW are very close to, but not the same as, those of RWGs. Specifically, the vias are shorted to both top and bottom metal planes of the substrate to provide vertical current paths. Consequently, the via pitch is an important parameter in SIW structures and it must be small enough to mimic the vertical metal walls of RWGs, otherwise the propagation characteristics of SIW will be significantly degraded.

The horizontal components of the surface current exist on the sidewalls for all TM modes and TE_{mn} modes with nonzero n's [63]. These horizontal current

paths will be cut in SIW structures, which results in radiation. That is why only TE_{m0} modes exist in SIW structures. After discussing and proving the similarity between SIW and RWG, empirical relations have been proposed between the geometrical dimensions of the SIW and the effective width a of the RWG with the same propagation characteristics. One of the most popular relations is [61].

$$a = w - \frac{d^2}{0.95s} \qquad (3.21)$$

An important aspect to consider when designing SIW structures is reduction of losses which is critical when operating at high frequencies. Just like RWGs, SIW structures would suffer from conductor and dielectric losses. Conductor losses (due to finite conductivity of metal walls) and dielectric losses (due to lossy dielectric material) in SIW can be estimated using classical equations in the literature used for RWGs. It is known that increasing the substrate thickness can significantly reduce conductor losses. The reason behind this is that for a given transmitted power, increasing the dielectric thickness reduces the amplitude of the electric current density flowing in the top and bottom metal layers, thus reducing the power dissipated [87]. In other words, the attenuation constant due to conductor loss is almost proportional to the inverse of substrate thickness. As for dielectric losses, they depend on the dielectric material as well as the geometry of the SIW structure; specifically, the SIW width [62].

3.9.2 Loss Mechanisms

A key issue in the design of SIW structures is related to loss minimization, which is particularly critical when operating at mm-wave frequencies. Three major mechanisms of loss need to be considered in the design of SIW structures, they are conductor losses (due to the finite conductivity of metal walls), dielectric losses (due to the lossy dielectric material) and possibly radiation losses (due to the energy leakage through the gaps). The behavior of conductor and dielectric losses is similar to the corresponding losses in rectangular waveguides filled with

a dielectric medium, and the classical equations can be effectively applied. Conversely, dielectric losses depend only on the dielectric material and not on the geometry of the SIW structure, and therefore they can be reduced only by using a better dielectric substrate. Finally, radiation losses can be kept reasonably small if $s/d < 2.5$.

3.9.3 Size and bandwidth

Another important topic to be accounted for in the design of SIW structures is the performance in terms of size and operation bandwidth. In fact, similar to rectangular waveguides, SIW structures are limited in compactness and bandwidth. The width of the SIW determines the cutoff frequency of the fundamental mode (with a reduction of factor $_r^{1/2}$ over hollow rectangular waveguides). The operation bandwidth is limited to one octave, corresponding to the mono mode bandwidth of the waveguide. The size and BW and their well-known tradeoff is already discussed in chapter 2's literature review.

3.10 CAVITY-BACKED PATCH ANTENNA

In the last few years, with rapid development of wireless communications, low profile antenna with good radiation performance and better isolation from feed network are in great demand, especially in space application such as satellite, aircraft, and radar. Cavity-backed patch antenna, for their attractive characteristics, are very suitable for those applications and have been studied by many researchers.

3.10.1. Patch Antenna

A patch antenna consists of a thin metallic patch, usually made of copper or gold, placed over a dielectric substrate which has a conducting ground plane at the bottom of it. Patch antennas have many profits like low profile, light-weight antennas most suitable for aerospace and mobile applications, they can be designed to operate over a large range of frequencies (1-40 GHz), easy integration

with linear or planar arrays and they can generate linear, dual and circular polarizations. More about MPA and their shape is already discussed in section 2.5.

3.10.2. Cavity-Backed Antenna

One of the most serious limitations of patch antennas is the narrow bandwidth. One solution is to increase the thickness of the substrate. However, thick substrate causes the propagation of surface wave. This is a serious problem in patch antenna because surface wave reduces the antenna efficiency and gain, limit the bandwidth, increase end-fire radiation, increase cross-polarization (XPL) radiation and limit the applicable frequency range. The radiation efficiency of the antenna decreases due to power carried away by the surface wave. To avoid these undesired effects, one of the suitable choices is to place the patch antenna into a metallic cavity to suppress the surface waves: cavity-backed antennas. The characteristics of cavity-backed antennas as reported in literature are summarized as follows:

- Cavities can suppress surface waves and mutual coupling in thick substrates and act as heat sinks in a high-powered large transmit array.

- Including stacked patch antenna configuration in a cavity further increases the bandwidth of patch antennas.

- Inclusion of high-permittivity superstrates on the cavity-backed patch antenna improves the antenna gain significantly.

- In a phased array antenna, cavities can prevent scan blindness, yield less coupling and improve good matching over wider scan angles.

- Gain and radiation patterns can be changed significantly by placing the patch antenna into a cavity enclosure and changing the shape of the enclosure.

- Patch with metallic cavity filled with dielectric material reduces the antenna dimensions. Up to 30% reduction in antenna diameter is achieved.

For those characteristics, a cavity-backed patch antenna was chosen, using SIW technology to suppress propagation of surface wave.

3.11 ARTIFICIAL MAGNETIC CONDUCTOR

3.11.1 Introduction

Artificial Magnetic Conductor (AMC) structures [65] also known as High Impedance Surface (HIS). One of the most interesting applications of AMC is in the design of efficient and low-profile antennas. Currently known AMCs are inherently frequency-selective and suffer from narrow band property which limits their applications in wideband or multiband antenna applications. The area of interest in this study is the investigation into the possibility of employing automatic optimization of elementary AMC cell geometry to tune its frequency characteristics i. e. its center frequency and bandwidth.

3.11.2 Methods

AMC is a type of metamaterial characterized by negative magnetic permeability. What is unique in AMC metamaterial is that phase reflection angle near to zero. Unlike normal electric conductors, the phase of the electromagnetic wave reflected on this artificial magnetic conductor is phase-shifted by an angle β of between −90° and +90° relative to the incident electromagnetic wave (in some other applications this range is limited to -45° and 45°) – see in Fig. 3.26. Of Course, this phenomenon only occurs for specific frequencies. The main goal of this research is to learn how we can control these frequencies.

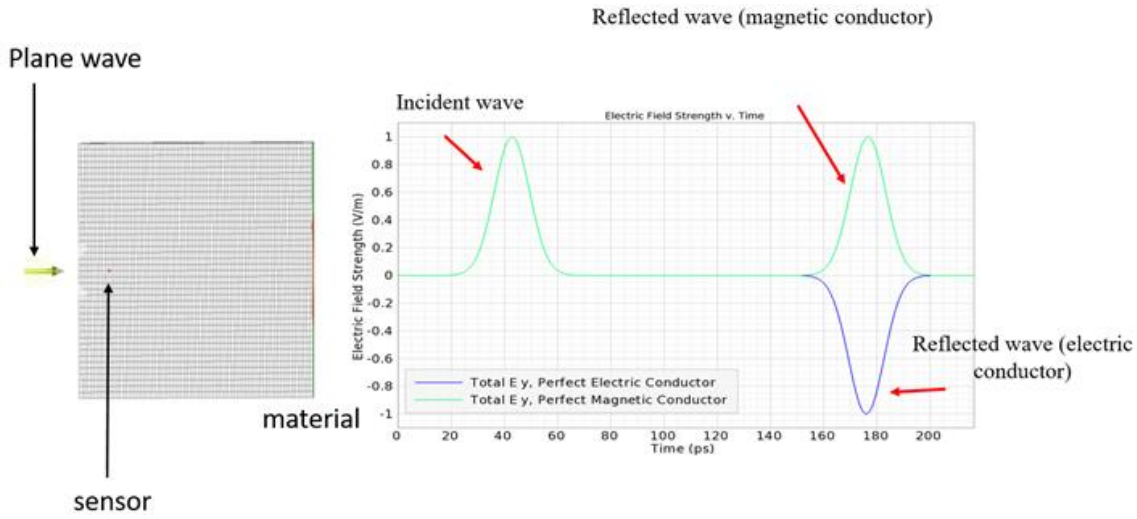

Fig. 3.26. Reflected wave characteristics: from normal, electric conductor and magnetic conductor [66]

Fig 3.27 presented general characteristics of μ-negative surfaces. In both cases the most important part is network of resonators (usually Split Ring Resonators (SRR) as resonator is used). Because a SRR may be described as a RLC circuit then SRR network also may be treated as network of coupled RLC circuits. Finally, meta-surfaces couple be modeled into two ways: using full electromagnetic simulations and circuit-based model.

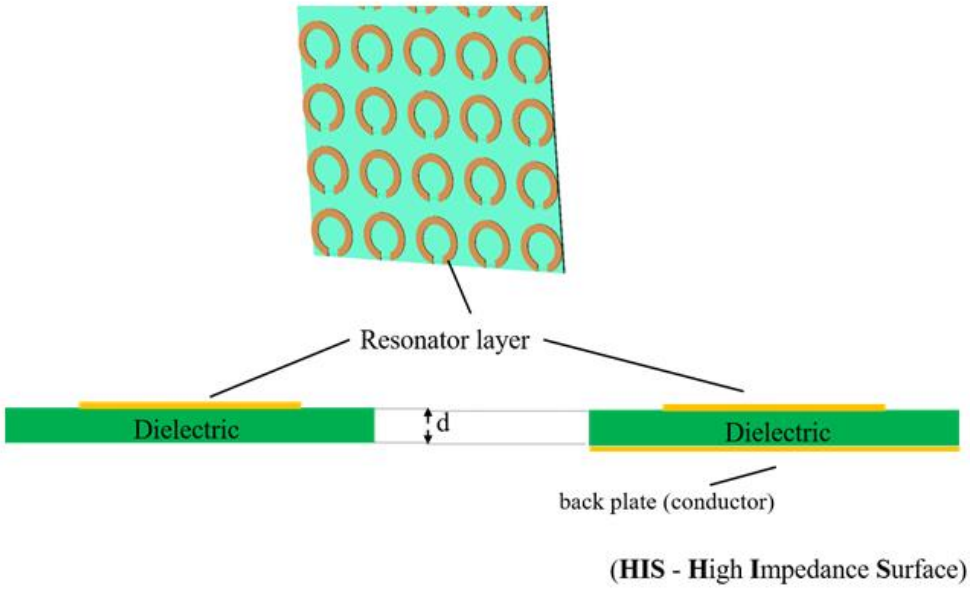

Fig. 3.27 General characteristics of μ-negative surfaces [66]

It should be observed that geometrical parameters of SRR are strong determine the electric properties of RLC circuit, particularly: radius and path width of SRR are determining of inductance of resonator (L_{in}), moreover gap with and path width are determining of gap capacity (C_g). From R, L and C parameters depend on characteristics of resonator, especially resonant frequency, and Q-factor (quality factor). in the case of resonators network, mutual (magnetic and electric) couplings they are also important. From the point of view of physical phenomena mutual coupling of two resonators results from the distribution of flux's - electric and - most of all - magnetic.

The goal of the optimization was to improve the AMC structure in terms of two objective function components: the bandwidth and the center frequency. This may be done in two ways: by geometry optimalisation with full field model or circuit-based model.

Chapter 4: The HMSIW Cavity-Backed Antenna with Patch's Array

4.1 INTRODUCTION

In this chapter, an HMSIW cavity-backed array antenna is proposed where the HMSIW cavity is used in conjunction with a patch antenna to improve further gain, BW, polarization authenticity, SLL, and efficiency. The whole patch antenna is further divided and based on the number of array elements in the patch, four array antenna cases have been proposed. A comprehensive investigation of them is presented. The proposed antenna operates at Ku-band, showing linearly polarized wave in TE_{101} mode and this hybrid combination provides several advantages. First, it has the advantages of a cavity-backed antenna and the conventional slot antenna. Second, an antenna is more compact. Third, it contains a much simpler matching network. In addition, being a member of the planner waveguide family, the proposed antenna also possesses a low profile and allows easy integration with the planner circuit. An exact representation of parameters of all antennas that have emerged during the designing course helps to grasp the sense of designing such kinds of hybrid array antenna of planner waveguide technology. Later, the proposed antenna is verified experimentally and exhibits a satisfying agreement with the data found during numerical simulation. A couple of experimental characterizations reveal this fabricated sample antenna to be a high gain antenna with wideband characteristics despite being small in size.

4.2 RESEARCH DESIGNS AND CONFIGURATION

4.2.1 Full Mode Square SIW

A typical rectangular size SIW is designed like Fig. 4.1(a), having a length and width designated by *L* and *W*. The SIW is designed on flexible Rogers RO4003C

(ε_r = 3.55, tanδ = 0.0027) having a thickness of h = 32 mil. The working frequency of TE_{mnp} represented SIW resonator can be calculated by the following [34]:

$$f_{mnp} = \frac{1}{2\pi\sqrt{\mu\varepsilon}}\sqrt{\left(\frac{m\pi}{L_{eff}}\right)^2 + \left(\frac{n\pi}{h}\right)^2 + \left(\frac{n\pi}{W_{eff}}\right)^2} \quad (4.1)$$

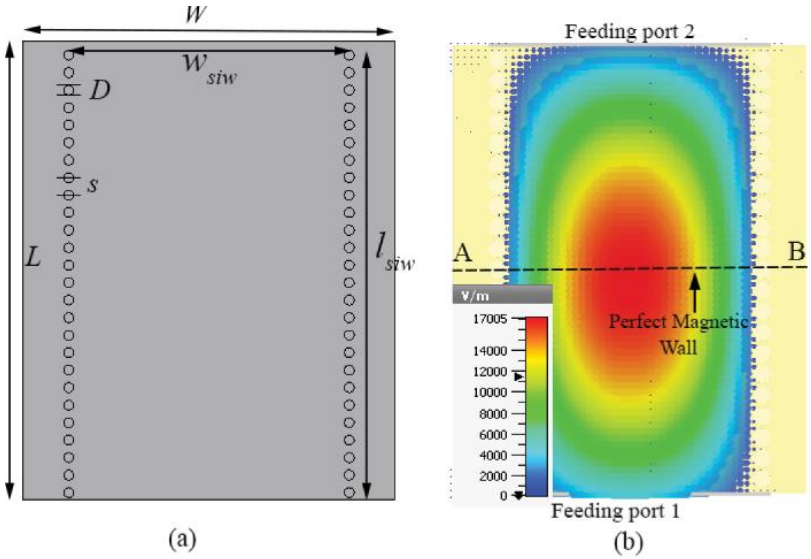

Fig. 4.1. Rectangular SIW resonator. (a) Full configuration. (b) Simulated electric field distribution at the fundamental frequency.

where m = 1, 2, n = 1, 2, …, p = 1, 2, …, $\mu = \mu_r\mu_o$, and $\varepsilon = \varepsilon_r\,\varepsilon_o$ indicates the permeability and permittivity of the chosen substrate of the SIW resonator, respectively. The equivalent length and width (L_{eff}, W_{eff}) can be determined by the following according to [9]:

$$L_{eff} = l_{siw} - 1.08\frac{D^2}{S} + 0.1\frac{D^2}{l_{siw}} \quad (4.2)$$

$$W_{eff} = w_{siw} - 1.08\frac{D^2}{S} + 0.1\frac{D^2}{w_{siw}} \quad (4.3)$$

In (4.2) and (4.3), D represents the diameter of via, and s represents the spacing between two adjacent via in SIW. Furthermore, some rules need to be fulfilled while designing SIW such as $s < 2D$ and $D/\lambda_0 \leq 0.1$, where λ_0 is the free space wavelength to maintain the device's longer life and acts as a conventional metallic cavity [9], [35]. In addition, the SIW possesses a large ratio of width to height that leads to n = 0 and resonates only TE_{m0p} modes. The electric field distribution of FMSIW in Fig. 4.1(b) is symmetrical along the AB plane and can

be considered a perfect magnetic wall (PMW). By dividing the rectangular SIW along the PMW, two semi-rectangular SIW (HMSIW) resonators with the same electric field are emerged.

4.2.2 Half-Mode Cavity-Backed Antenna

The emerged HMSIW radiates through the substrate named as dielectric aperture depicted in Fig. 4.2. Since the electric field distribution is half of that fundamental TE_{101} mode, it is called HMSIW. Though electric field distribution is halved, its operating frequency are nearly identical. Small shifting can be ignored. Thus, HMSIW can reduce its size. The HMSIW operates at 13.35 GHz of Ku-band, having a BW of 170 MHz, and the radiation efficiency, about 70.7%, gives a clue of loss within the antenna structure in Fig. 4.3. The simulated

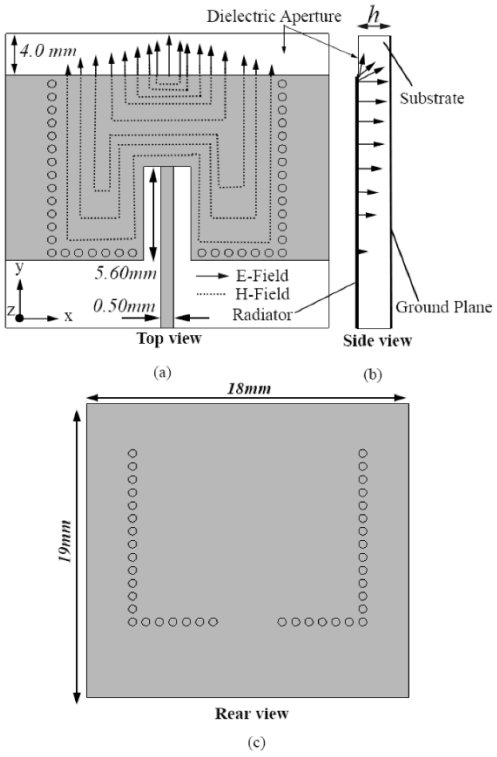

Fig. 4.2. Layout of HMSIW antenna. (a) Top view with magnetic field distribution. (b) Side view with electric field distribution (h = 32 mil). (c) Rear view.

normalized radiation pattern at 13.35 GHz for HMSIW is shown in Fig. 4.4(a). The antenna has a cross-polarization level (XPL) of less than −13.0 dBi, with a net gain of 6.8 dBi, and its main beam points in a boresight direction of $\varphi = 13°$. Half power beam widths (HPBWs) for this HMSIW cavity-backed antenna are 80° and

64° in E-plane (E_θ in $\varphi = 90°$) and H-plane (E_φ in $\varphi = 0°$), respectively. Furthermore, the antenna's beamwidth in the azimuth plane is narrower than in the elevation plane due to the width of the radiating aperture of the antenna. The operating principle of this HMSIW is very similar to that of the presented triangular-HMSIW in [13] and semicircular HMISW in [33], while the proposed one is a semi-rectangular cavity. In [13], the input port had been designed to be parallel to PMW, and it emerged as a triangular HMSIW cavity, unlike this proposed one where the input port is perpendicular to PMW. Another QMSIW is proposed [19], where the antenna was cut twice along PMW, parallel and perpendicular to the input port. By cutting the antenna twice along PMW, the antenna emerges as QMSIW. In addition, orthogonal degenerate modes (ODMs) were generated by optimizing the two radiating edges, unlike in [13], where the antenna shows LP.

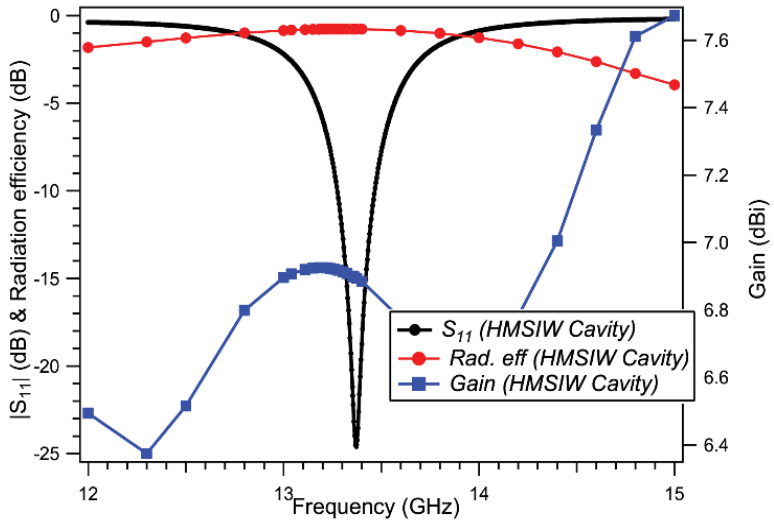

Fig. 4.3. Return loss, gain and radiation efficiency of HMSIW cavity antenna over its working frequency.

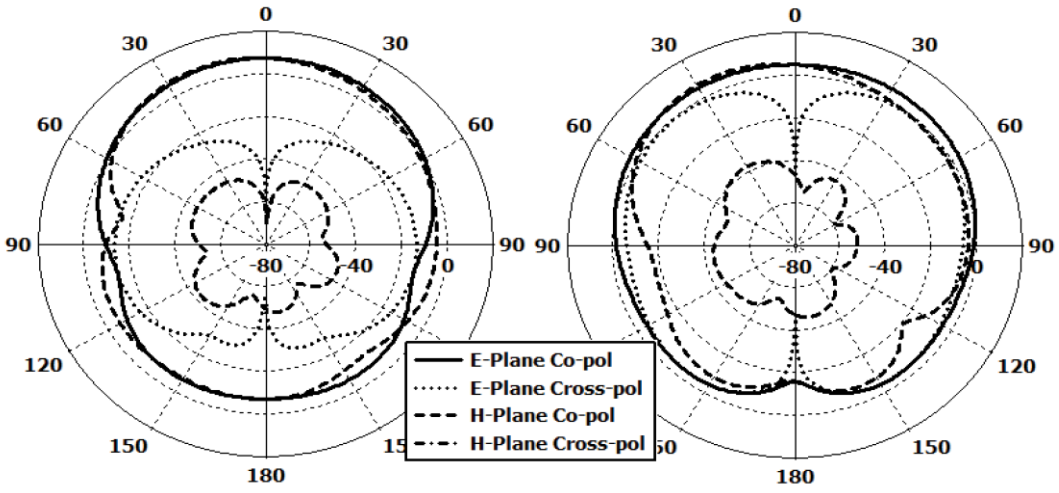

Fig. 4. 4. Normalized radiation pattern with XPLs. (a) HMSIW antenna at 13.35 GHz. (b) Hybrid antenna at 13.19 GHz.

4.2.3 Hybrid Antenna

The addition of a patch in Fig. 4.5 causes to decrease the antenna's overall resistance. Therefore, to control input impedance, the inset feed's length and width are shortened and widened, respectively. For the best response, the suitable dimension of the patch was chosen by using (4.4) and (4.5) [36]. In this case, this is a parasitic patch since it is not directly connected with the main feed line.

Additionally, QMSIW has couples of higher-order modes where circular polarization (CP) comes in TE_{202} mode for ODM. Needless to say, every mentioned [13], [19], [33] antenna radiates in a very similar manner to this proposed HMSIW through the substrate, known as radiating aperture, of their original cavity's mode. Note that these antennas suffer from low BW because of the high *Q*-factor contributed by cylindrical vias on their structure. In Fig. 4.6, TE_{101} mode electric field and its magnetic current distribution for the patch are shown. It assumes the electric field is uniform across substrate height, $d/dz \approx 0$, but varying sinusoidally across both the length and width of the patch unlike the patch proposed in [33]. The patch in [33] got excited by their original TE_{010}

fundamental mode of the circular cavity where the electric field varies sinusoidally in one direction. In addition, both of these patches get excited by their original cavity's mode, and their operating frequency has been merged for possible BW escalation. This proposed hybrid antenna radiates its fundamental mode in a very similar way to the antenna in [33] through the substrate. Note that this cancellation of the electric field on both sides of the patch in Fig. 4. 6 causes elevated XPL in the boresight direction compared with the HMSIW antenna, which is vivid from Fig. 4.4(b).

$$W_P = \frac{c}{2f_{rp}}\sqrt{\frac{2}{(\varepsilon_r+1)}} \tag{4.4}$$

$$L_P = \frac{c}{2f_{rp}\sqrt{\varepsilon_{re}}} - 2\Delta L \tag{4.5}$$

In (4.4) and (4.5), f_{rp} indicates the same resonant frequency of the patch excited by mode TE_{101}, where re refers to effective permittivity and L means extended incrementally length patch [36]. The resultant RC, gain and radiation efficiency of the hybrid antenna are shown in Fig. 4.7, where antenna BW enhancement is noticeable with a come down in gain from 6.8 to 5.5 dBi. Howbeit, the radiation efficiency points higher than the HMSIW cavity antenna. The normalized radiation pattern of both E- and H-plane with XPL for a hybrid antenna are shown in Fig. 4.4(b). The E-plane (E_θ in $\varphi = 90^\circ$) pattern is symmetrical; however, H-plane is antisymmetric and has shifted to 24◦ from the boresight direction as shown in Fig. 4.4(b). The HPBW in E- (E_θ in $\varphi = 90^\circ$) and H-plane (E_φ in $\varphi = 0^\circ$) are 136.6◦ and 55.4◦ respectively.

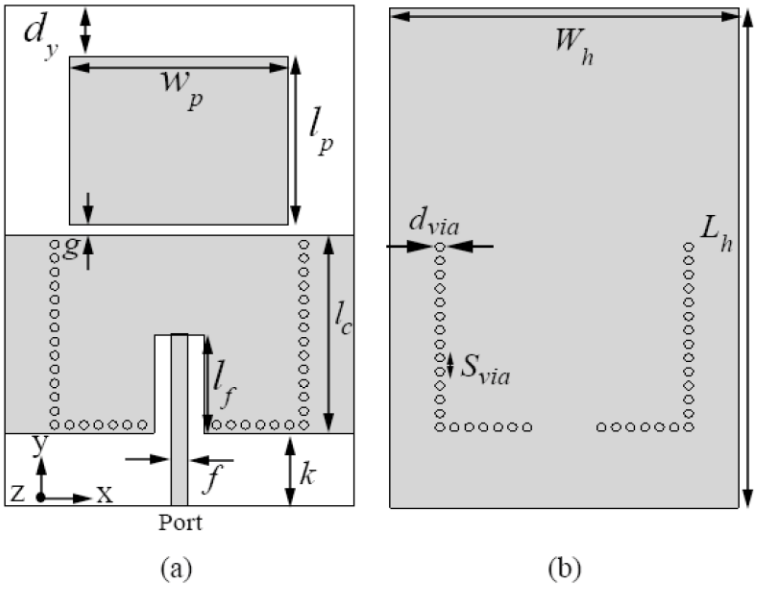

Fig. 4. 5. Complete layout of the hybrid antenna. (a) Top view and (b) rear view where L_h = 25.50 mm, W_h = 18 mm, d_y = 2.6 mm, w_p = 11.10 mm, d_{via} = 0.45 mm, S_{via} = 0.75 mm, l_p = 9.10 mm, g = 0.53 mm, l_c = 10.70 mm, l_f = 5.30 mm, f = 0.80 mm, and k = 3.9 mm.

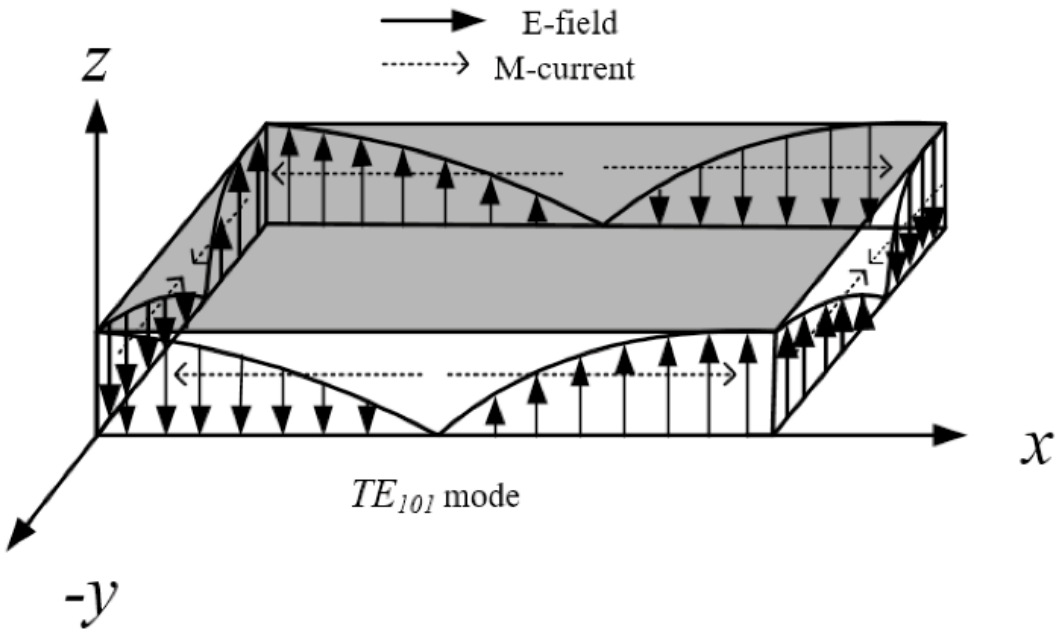

Fig. 4. 6. Electric field and magnetic current distribution of patch for TE_{101} mode.

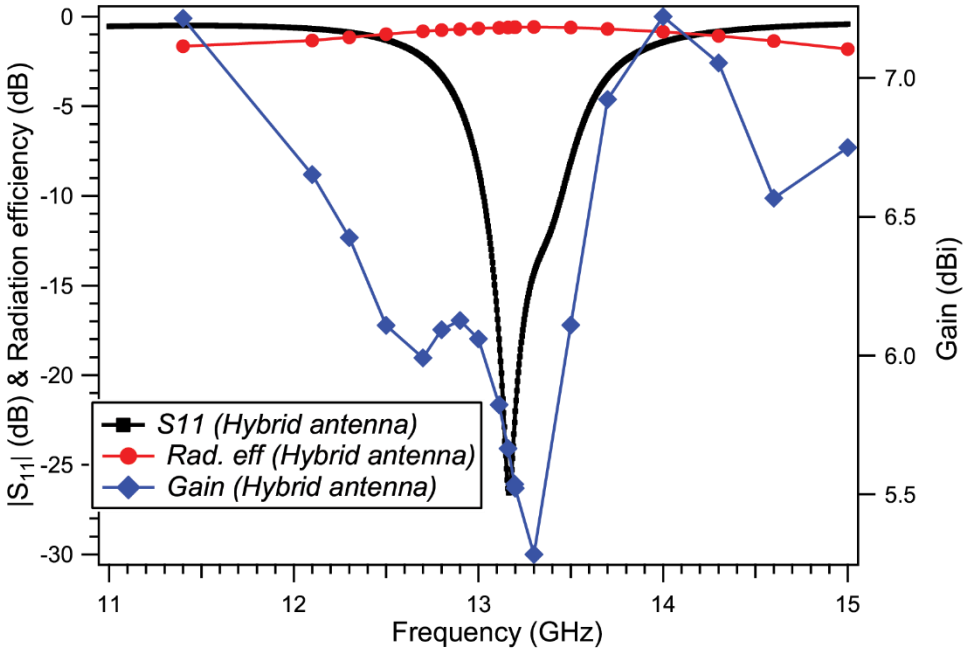

Fig. 4.7. Return loss, gain and radiation efficiency of hybrid antenna over its working frequency.

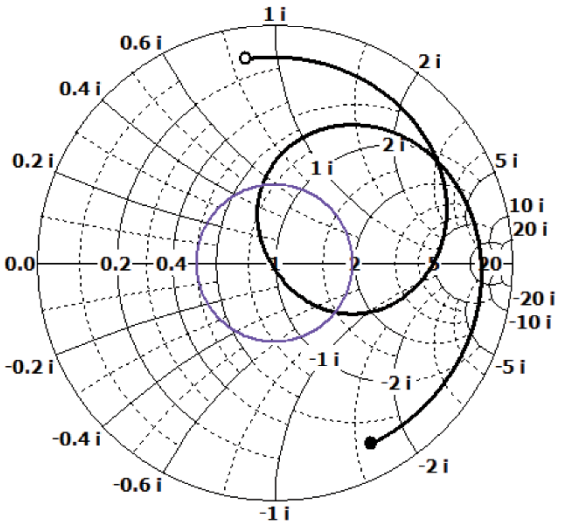

Fig. 4. 8. Simulated antenna input impedance view of hybrid antenna.

A loop appears in the Smith chart in Fig. 4.8 due to the coupling between the patch and cavity-backed antenna, which is partially inside the VSWR = 2 circle. It reveals perfect impedance matching since it passes over the prime centre. In addition, the size of the loop depends typically on the width of the patch, and the coupling between the patch and cavity and its size inside VSWR = 2 circles determines antenna impedance BW.

4.3 THE PROPOSED HYBRID ARRAY ANTENNAS

The patch has been divided into a couple of parts, where every small part act as a small resonator. About 0.2 mm of separation exists between each array of elements of the antenna. This division finally introduces several new possible structures illustrated in below in Fig. 4.9. Each array element has the same size resulting in working asthe same resonator of a particular frequency where side walls act as a magnetic wall. Furthermore, these elements are getting excited by the cavity resonator through radiative coupling, and this near-field coupling determines the phase and amplitude of the sidewalls of each array element. They are designed to radiate and occupy the quality factor in the same order as that of the antenna's driven element. The resultant electric field of the antenna in the far-field region would be the summation of both array elements and cavity resonator.

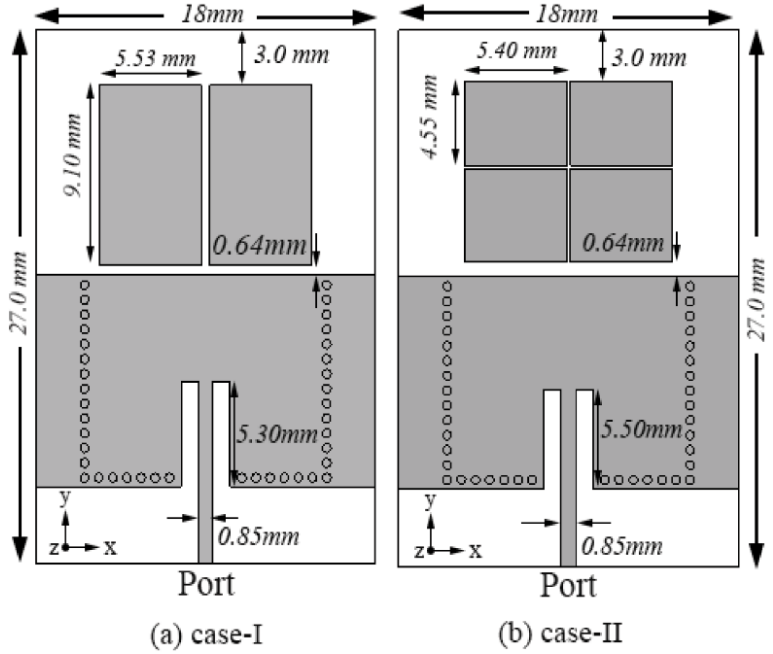

Fig. 4.9. Layout of cavity-backed hybrid array antenna. (a) Case-I. (b) Case-II.

Total electric field E array of the array elements can be figured out with the help of (4.6) by adding up the electric field of each array element [37].

$$\vec{E}_{array}(\theta,\varphi) = \sum_{P=1}^{P} a_p \vec{E}_p(\theta,\varphi) e^{jk\hat{r}r_p} \qquad (4.6)$$

where $\vec{E}_P$ is a complex linearly polarized radiative field radiated by each element (active element pattern including the mutual coupling), a_p is the

complex excitation coefficient, $\hat{r}$ is the unit vector in the direction of far-field (θ, φ), wavenumber $k = 2\pi/\lambda$, and p is the array element number

4.3.1 Two Parasitic Patches (Case-I):

Case-I emerged by dividing the parasitic patch into equal two halves are depicted in Fig. 4.9(a), which are getting excited through magnetic coupling with a gap of 0.64 mm. The slot has been divided into two parts that increase the antenna aperture area. This increment in aperture area escalates antenna radiation while decreasing its overall impedance. Therefore, feed linewidth has been increased, which is 0.85 mm in this case-I. The identified loop in impedance loci of the antenna is partially inside the VSWR = 2 circle in Fig. 4.11(a). The loop becomes mildly smaller due to weaker coupling and finally gives rise to an increase in BW slightly from 380 to 398 MHz for VSWR ≤ 2. However, BW is not optimum. The gain in both planes is decreased because the sidelobe appears more substantial than the previous structure. It is because newly divided patches have experienced a phase delay with respect to the feeding port. decreased because the sidelobe appears more substantial than the previous structure. It is because newly divided patches have experienced a phase delay with respect to the feeding port.

4.3.2 Four Parasitic Patches (Case-II):

In Case-II, the patch has been divided into four halves in Fig. 4.9(b), resulting in a significant increase of around 7.02 dBi due to an increase in aperture area. The antenna's overall resistance again decreased, and to match the impedance, the inset feed length has been lengthened. However, the coupling gap was kept as same as before. The parasitic patches have been given the same size, which resonates in the vicinity of the cavity-backed antenna resulting in an increase in BW that is most out of four cases. In this case, radiation is increased inside the cavity antennas, reducing the quality factor reported in Table 4.1. The identified

loop in impedance loci of the antenna is partially inside the VSWR = 2 circle in Fig. 4.11(a) becomes mildly smaller again due to weaker coupling. This finally gives rise to an increase in BW slightly from 398 to 425 MHz for VSWR ≤ 2.

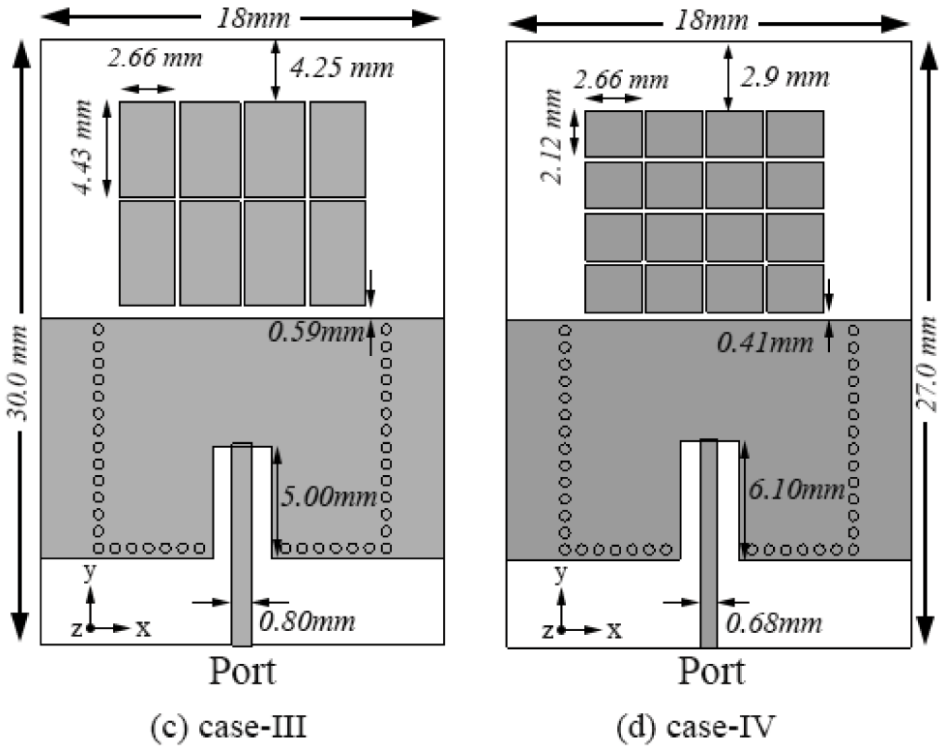

Fig. 4. 10. Layout of cavity-backed hybrid array antenna (c) Case-III. (d) Case-IV.

However, again it's not optimum BW. The main beam points at 37° boresight direction and introduces a sidelobe which is most out of four cases that gives rise to power wastage. The E-plane (E_θ in $\varphi = 90°$) gain, therefore, has decreased. Furthermore, the gain of H-plane (E_φ in $\varphi = 0°$) increased considerably irrespective of huge sidelobe levels (SLLs) of the antenna. The HPBW gets narrowed most out of four cases in this plane which helps to concentrate the beam in one direction. The XPL in E-plane (E_θ in $\varphi = 90°$) is positive, leading to a slightly lower radiation efficiency than case-I (Table 4.1).

4.3.3 Eight Parasitic Patches (Case-III):

The edge of the radiating patch has been divided into four parts leading the antenna to have a weaker coupling and impedance matching. The gap coupling

is reduced to match the impedance by keeping the length and width are same as in the previous case. In this case, the fundamental frequency of the parasitic resonator has shifted from the vicinity of HMSIWs operating frequency causing no further escalation of impedance BW. Furthermore, the loop in the smith chart is partially inside into VSWR = 2 circles, giving rise to a decrease in BW of 330 MHz for VSWR ≤ 2 than the cases-I and II. Each parasitic patch's gain dramatically contributes to the antenna's overall gain after increasing the aperture area.

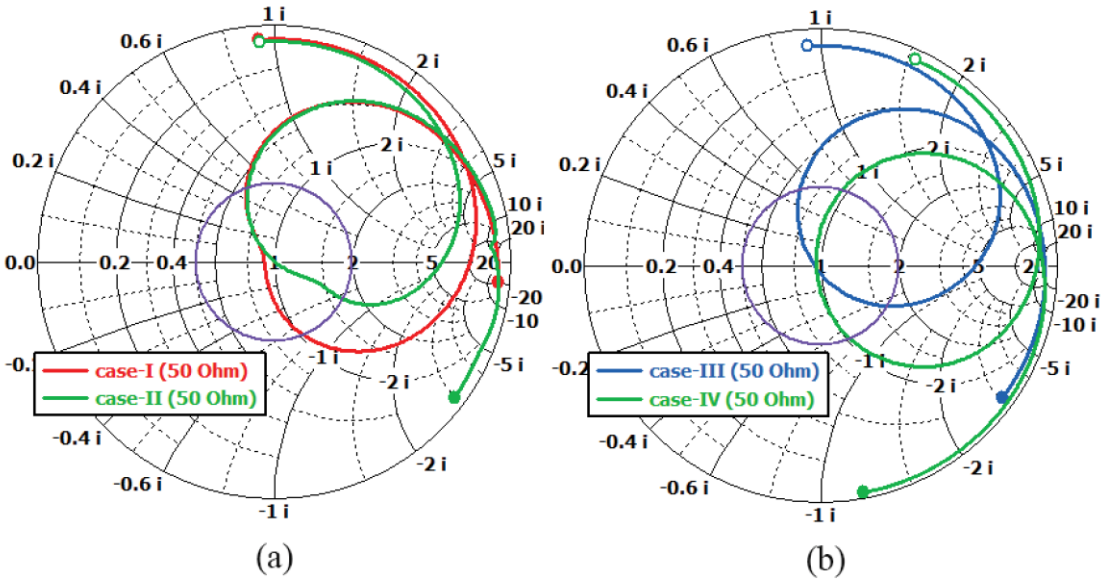

Fig. 4. 11. Simulated input impedance view of all four cases of antenna. Smith chart for (a) case-I and case-II and (b) case-III and case-IV antenna.

It gives rise to an enhanced gain of 8.95 dBi in both planes with minimized SLLs. In addition, the H-plane (E_φ in $\varphi = 0°$) gain has been spotted to be the maximum out of four cases. In this case-III, the antenna shows good minimized XPL levels at each plane that elevates antenna net gain, especially in H-plane (E_φ in $\varphi = 0°$).

TABLE 4.1 PERFORMANCE COMPARISON OF ALL FOUR CASES OF ANTENNA

Parameters	**Cases**			
	Case-I	**Case-II**	**Case-III**	**Case-IV**
Working freq.	13.196GHz	13.385GHz	13.38GHz	13.275GHz
BW	398 MHz	425 MHz	330 MHz	194 MHz
VSWR	1.02	1.01	1.02	1.03
Gain	4.79 dBi(E) 4.25 dBi (H)	4.29 dBi (E) 7.02 dBi (H)	4.68 dBi (E) 8.95 dBi (H)	7.24 dBi (E) 8.18 dBi (H)
SLL	-6.2 dB(E), -8.7 dB(H),	-5.1 dB(E), -6.2 dB(H)	-8.10 dB(E), -7.50 dB(H)	-12.2 dB(E), -10.0 dB(H)
XPL	2.24 dBi (E) -7.5 dBi (H)	2.93 dBi (E) -11.9 dBi (H)	-14.1 dBi (E) -17.7 dBi (H)	-9.48 dBi (E) -16.1 dBi (H)
Realized gain	1.4 dB(E), 3.51 dB(H)	3.45 dB(E), 6.29 dB(H)	4.17 dB(E), 8.51 dB(H)	4.50 dB(E), 7.19 dB(H)
Beam direction	36° (E),18° (H)	37°(E),29° (H)	0° (E),32° (H)	0°(E),15° (H)
HPBW	147.6°(E),109.5°(H)	144.2°(E), 50.6°(H)	63.7°(E),60°(H)	76.9(E),55.3°(H)
E-field	17.4 dBV/m	18.5 dBV/m	23 dBV/m	21.9 dBV/m
H-field	-34.1 dBA/m	-33.1 dBA/m	-28.5 dBA/m	-29.6 dBA/m
Radiated Power	0.42136 W	0.4221 W	0.42158 W	0.3983 W
Copper loss	0.0177 W	0.0158 W	0.01568 W	0.0261 W
Dielectric loss	0.052 W	0.055 W	0.046 W	0.058 W
Accepted power	0.475 W	0.481 W	0.478 W	0.470 W
Q-factor	33.07	32.55	41.17	68.42
Q_R	37.28	37.54	46.61	81.0
Rad. eff.	88.73%	86.66%	88.28%	84.37%
Total eff.	84.27%	84.62%	84.32%	79.36%

Moreover, the antenna also exhibits the highest realized gain among the four cases with the lowest dielectric loss. The E-plane (E_θ in $\varphi = 90°$) radiation is symmetrical, having a narrower HPBW to boresight axis. However, H-plane (E_φ in $\varphi = 0°$) is asymmetrical; it is due to parasitic array elements that are placed on X-axis direction experienced phase delay with respect to the feeding location.

4.3.4 Sixteen Parasitic Patches (Case-IV):

A high gain of 8.18 dBi was achieved with minimized SLLs of −12.2 dB by dint of dividing the patch layer into 16 equal small patches. The HPBW in H-plane (E_φ in $\varphi = 0°$) is reduced dramatically reported in (Table 4.1). An increased number of parasitic patches provide some radiation in X-direction and increase the aperture area. The gap coupling is reduced to 0.41 mm, giving rise to a stronger coupling and antenna obtains a larger loop in impedance loci out of four cases in Fig. 4.11(b). In addition, the antenna obtains the lowest BW of 194 MHz (2.9%) for VSWR ≤ 2. Notwithstanding possessing the smallest BW, it shows a better degree of polarization purity in terms of both E- (E_θ in $\varphi = 90°$) and H-plane (E_φ in $\varphi = 0°$) with less than −9.5 dBi XPL. None of those mentioned above cases obtained optimum BW. Furthermore, the case-IV antenna meets the highest dielectric and copper loss which coerced the antenna to accomplish an efficiency of 79.36%, which is the lowest among the four cases

$$1/Q_l = 1/Q_u + 1/Q_e = 1/Q_R + 1/Q_c + 1/Q_d \quad (4.7)$$

$$Q_u = f_r/\Delta f_{7dB} = \eta_R Q_R. \quad (4.8)$$

The unloaded quality factor (Q_u) of the proposed structure that describe the damping and internal losses of the cavity, rely on radiation (Q_R), copper (Q_c) and dielectric (Q_d) quality factor of the antenna (4.7) where external quality factor (Q_e) remains ineffectual. It can also be calculated by (4.8), where f_{7dB} represents a band of frequency where the amount of power reflection is not more than one-fifth (−7 dB) of that absorbed at fr in matching condition [38]. The gain, and XPL of both E-plane (E_θ in $\varphi = 90°$) and H-plane (E_φ in $\varphi = 0°$) of all four cases antenna

are mentioned in Table 4.1. It is sensible that the polarization purity is upward with an increasing number of parasitic patches. In comparison with case-I and case-II, the rest of the two antennas have better polarization purity with high gain (Table 4.1). In case-II, the antenna shows wideband behaviour with lowest the quality factor where its Q_R is supposed to be the lowest among all cases. Still, due to degradation in radiation efficiency, Q_R of case-II calculated by (4.8) is higher than case- I (Table 4.1). This degradation of radiation efficiency is due to elevated XPL in E-plane of case-II. Clearly, from Table 4.1, case-III and case-IV antenna stand out.

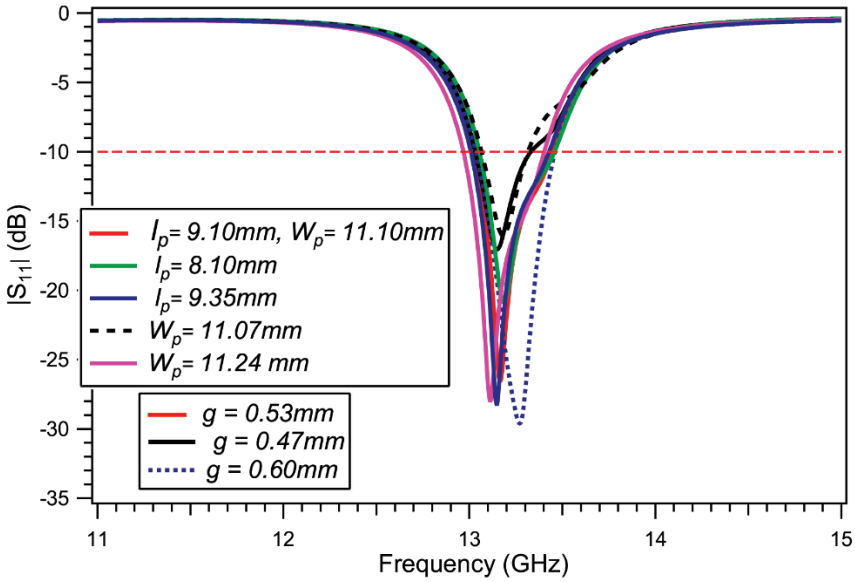

Fig. 4. 12. Effect of coupling gap g, patch width W_p and length l_p on reflection characteristics curve of hybrid antenna.

4.4 THE PARAMETRIC STUDY

A couple of simulations have been carried out in CST to examine the effect of different parameters on the antenna's performance. The results are displayed in this section in phases.

4.4.1 Effect of g, W_P and l_P on Reflection Coefficient

Fig. 4.12 implies the patch's effect on BW and the impedance matching. Not only the gap coupling *g* but also a suitable patch's dimension was chosen for the

hybrid antenna after several simulations to get the best response from the antenna.

4.4.2 Effect of Dielectric Length on SLL, Gain and Radiation Efficiency

Antenna's gain was supposed to be elevating with increasing dielectric length; however, case-IV shows a de-escalation as the SLL curve vehemently upward Fig. 4.13. It is due to SLL causes wastage of input power. Actually, the antenna behaviour of case-III is antithetical to case-IV. In case-III, antenna gain is upward with increasing DL, hence a DL of 5.75 mm was chosen, which is most among all cases shown in Fig. 4.10(c). Note that when DL is upward for the case-IV, the

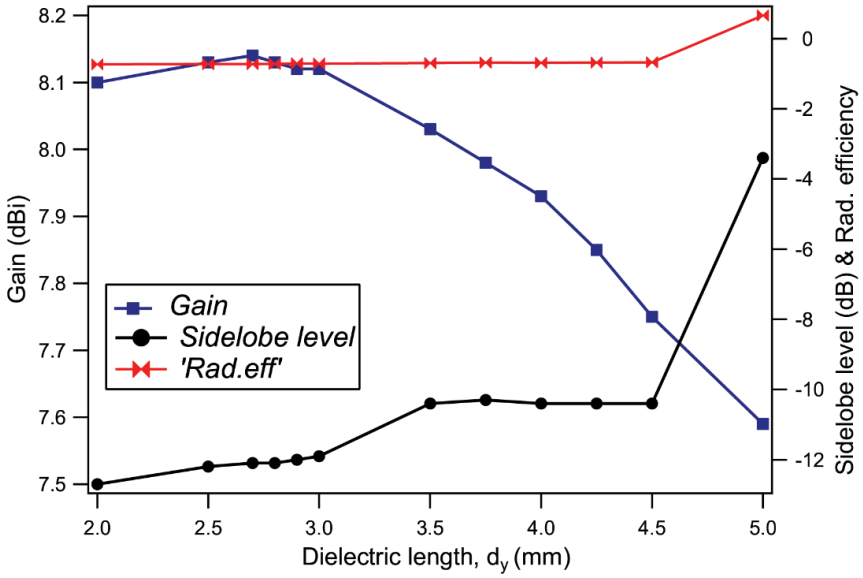

Fig. 4. 13. Effect of dielectric length on SLL, gain and radiation efficiency of the case-IV antenna at its resonant frequency.

antenna's main beam is more prone to shift from the boresight axis due to phase shift with respect to the feed patch that aggravates the SLL. The antenna radiation efficiency curve is also upward in Fig. 4.13 for case-IV because XPL is less dominant with an increment of DL.

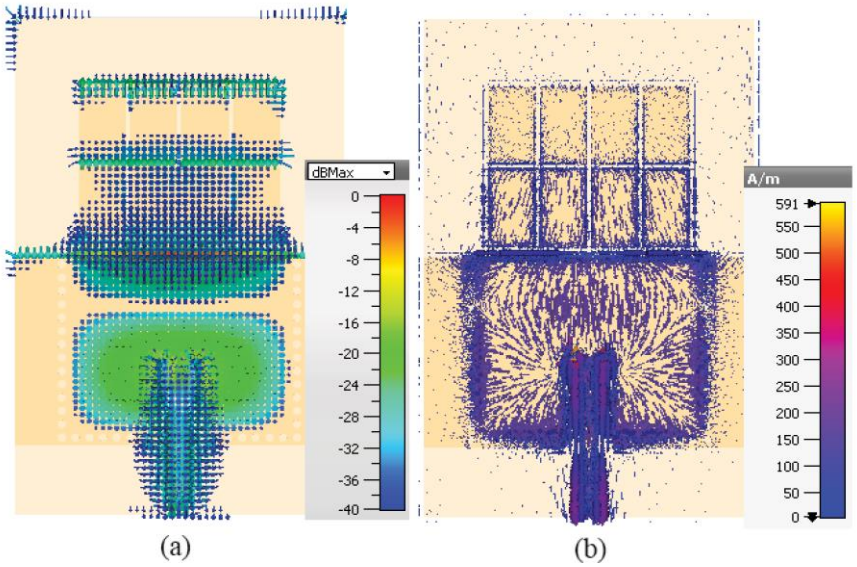

Fig. 4. 14. Simulated parameters of case-III antenna. (a) Electric field distribution and (b) current distribution with appropriate color map at 13.38 GHz.

4.4.3 Electric Field and Surface Current Distribution

The simulated E-field distribution for TE_{101} mode in Fig. 4.14(a) is a mirror of good coupling between a cavity-backed antenna and parasitic patches. Besides, simulated current distributions in Fig. 4.14(b) ensure that the whole antenna takes part in resonating by electromagnetic coupling. The magnetic current on every patch can be calculated from the cavity model reported in [39].

4.5 THE EXPERIMENTAL VALIDATION

The proposed case-III antenna is fabricated, shown in Fig. 4.15 and tested using a vector network analyzer (VNA) to verify its theoretical analysis. The substrate Rogers R04003 of 32 mil thickness is used as a substrate to fabricate the antenna. The measured return loss (S_{11}), which is compared with both CST and full-wave HFSS simulation, is shown in Fig. 4.16. The measured return loss (S_{11}) has many similarities with the simulated one; first, it covers the operating frequency range of CST simulated S_{11} after obtaining 160 MHz more BW than CST S_{11} in Fig. 4.16.

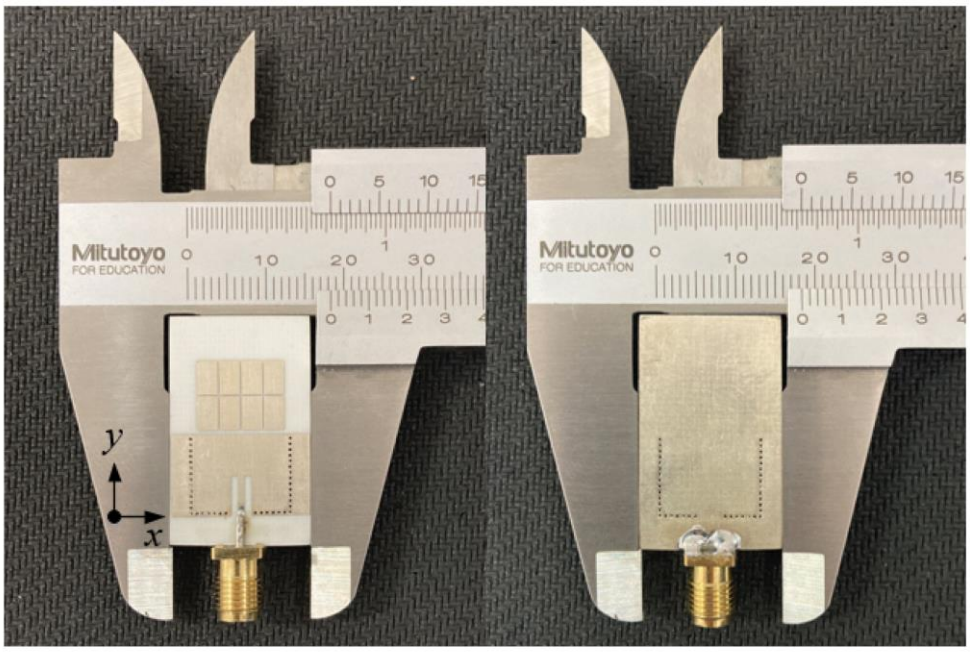

Fig. 4. 15. Photograph of the fabricated proposed case-III antenna with the slide caliper (mm) (a) Front view and (b) rear view.

Second, the measured return loss has a BW of 490 MHz ranging from 13.03 to 13.51 GHz while obtaining an RC value better than −45 dB at 13.32 GHz, indicating excellent impedance matching. Eventually, the BW was supposed to be in the vicinity of 330 MHz as per CST simulation. The increment in BW Fig. 4.16 is the inevitable

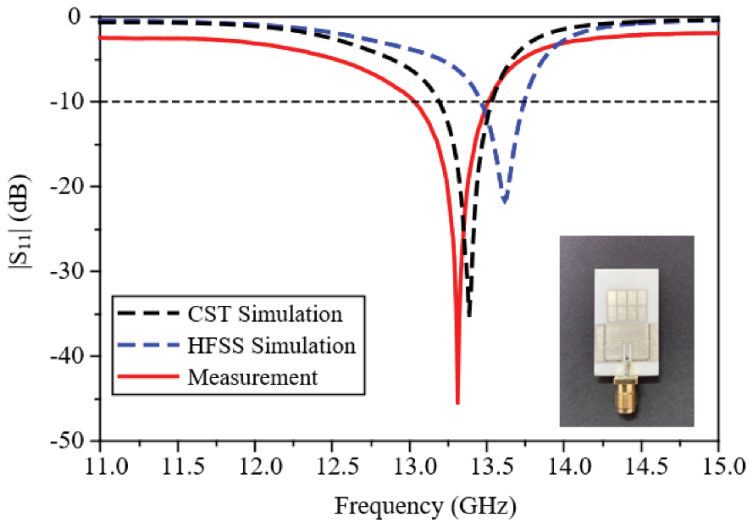

Fig. 4.16. Measured return loss of proposed case-III array antenna in comparison with both CST and HFSS.

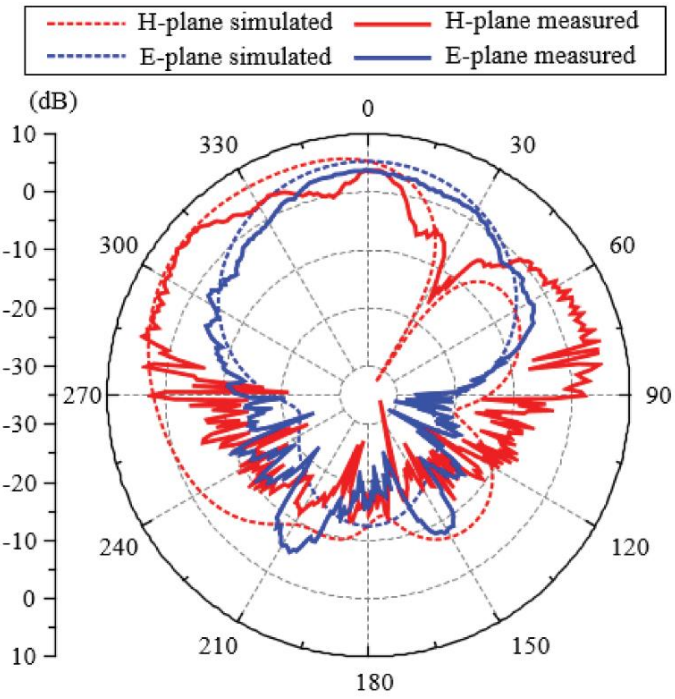

Fig. 4. 17. Measured and simulated H-plane (XZ cut) and E-plane (YZ cut) radiation patterns of case-III at 13.32 GHz.

outcome of reducing the *Q*-factor caused by introducing loss in the system. Some losses such as SMA connector loss, conductor loss which is replaced by to speed up the simulation, and soldering loss effects are voided in numerical simulation. These parameters introduce loss during the measurements process resulting in a degradation in the antenna's *Q*-factor. In addition, soldering loss leaves an indelible effect on *Q*-factor and is considered the main contributor to ohmic loss inside the antenna. As a result, the de-escalation in *Q*-factor is so dominant that the measured BW for the case-III antenna is the highest out of four cases (Table 4.1), making this case-III antenna a wideband antenna. Furthermore, the resonant frequency shifting prevails for fringing effect and fabrication imperfections such as inaccuracy in the air gap between patches.

Meanwhile, all the mentioned loss inside the antenna affects realized gain, XPL, and other parameters of the antenna that will be discussed in the following. The far-field realized gain radiation pattern of the case-III antenna is shown in terms of E- (E_θ in $\varphi = 90°$) and H-plane (E_φ in $\varphi = 0°$) were tested at the anechoic chamber of Hanoi University of Science and Technology. The radiation pattern

in Fig. 4.17 is compared with CST simulated pattern, and many similarities were found to that of predicted simulated data in Section II. In particular, the measured realized gain in both E- and H-plane renders many similarities to that of the simulated one reported in Table 4.1. The measured E-plane realized gain is 3.90 dB, whereas the simulated gain was 4.17 dB (Table 3.1, column 3, row 7). Similarly, the measured H-plane realized gain was 7.97 dB, a bit lower than the simulated gain of 8.51 dB. It was due to an undesirable increment in BW.

Moreover, due to the ohmic loss mentioned previously, *Q*-factor comes down, affecting antenna net gain and reducing antenna efficiency. As an escalation in BW happens undesirably, antennas realized gain per se decreased accordingly to maintain energy conservation. This relationship between BW and gain has been a well-known trade-off for the antenna. The measured E-plane is symmetrical and points at 0° boresight direction in Fig. 4.17, which is like the simulated one reported in Table 4.1. In contrast, the H-plane slightly shifted from the boresight direction due to phase shift with the feed point already predicted in simulation (Table 4.1). The measured HPBW in both E- and H-plane were 59° and 33°, respectively.

The E-plane HPBW maintains a satisfying agreement with E-plane simulated HPBW value mentioned in Table 4.1. Here, the H-plane leading beam with a single lobe that was spotted in the simulation gets divided between two major lobes due to fabrication imperfection. Therefore, HPBW gets distorted more than the simulated one (Table 4.1). The proposed antenna is asymmetrical in XZ-plane, and an inaccurate air gap between parasitic patches in the fabricated sample introduces more asymmetricity in XZ-plane. Therefore, two major lobes have appeared in the H-planes pattern. The H-plane gets slightly distorted in shape compared to the simulated one. This distortion in shape periodically brings out a discrepancy on the sidelobe at H-plane compared to its corresponding simulation value. Despite the distorted H-plane radiation pattern, the antenna achieves a high realized gain of 7.97 dB, almost in the vicinity of simulated data,

which meets the expectation of being an array antenna. In addition, the measured E-plane SLL is −7.25 dB, and the simulated SLL is −8.10 dB, as reported in Table 3.2, indicating good agreement. A nugatory difference of 0.85 dB for the E-plane's SLL was reported. However, a difference of more than 2.0 dB in the H-plane's SLL appeared during measurement. It is because fabrication fault, as discussed earlier, introduces this deviation in SLL. Additionally, spurious radiation from the feed line could aggravate the SLL level.

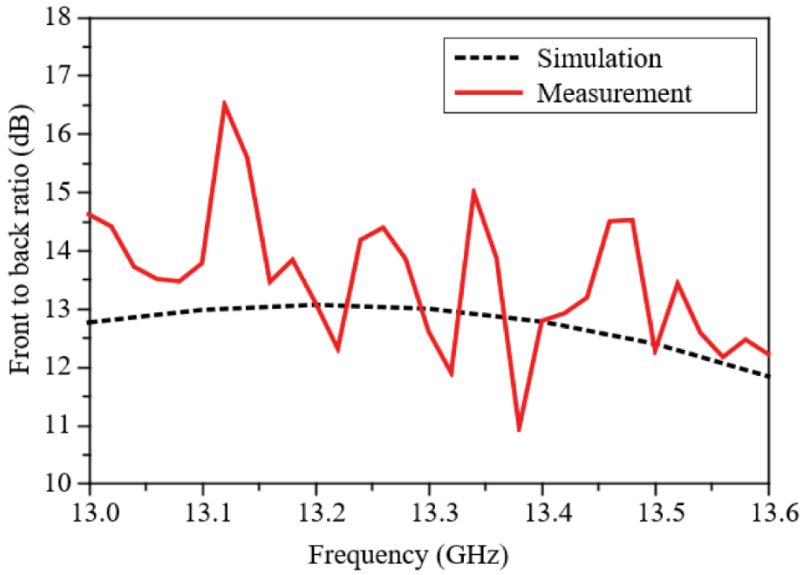

Fig. 4.18. Simulated and measured front to back ratio of proposed case-III antenna over its frequency range.

Nonetheless, placing the feed line on the ground plane could reduce spurious radiation up to a level. The measured XPL, not included in Fig. 4.17 for a simple visual representation of antennas radiation pattern, was found to be less than −11.0 dB for E-plane and less than −13.0 dB for H-plane.

Furthermore, the measured XPL on both planes were spotted to be higher than that of the simulated XPL reported in Table 4.1. Therefore, it implies antenna meets loss within it, as discussed already, which pushed the XPL level up and slightly spoils the polarization authenticity. The ripple is visible in the measured radiation pattern, which indicates a continuous 180° phase shift of surface current by the PEC ground plane with respect to the radiator. However, this can be overcome by using a meta-surface, known as high impedance surfaces as

superstrate [40], which will also help increase both gains, front to back ratio (FTBR), and SLL. The FTBR for the proposed fabricated sample has been measured and compared with simulated ones in Fig. 4.18. The measured FTBR varies from 15 to 11 dB over its frequency range, while simulation shows a stable response in the vicinity of 13 dB. Clearly, the measured FTBR was almost 12 dB at 13.32 GHz, whereas the simulated FTBR was 12.8 dB. A slight deviation of 0.80 dB exists compared to numerically simulated data.

In addition, a planar dogbone-shaped meta-surface (MS) is proposed and shown in Fig. 4.19(a). The dogbones metasurface is also known as high impedance surface (HIS), an anisotropic MS, which is backed by a perfect electrical metal sheet. The meta-surface is primarily designed to operate at 2.42GHz, i.e., it provides an in-phase reflection at 2.4GHz. As the HMSIW radiates TE_{110} linearly polarized wave, the meta-surface was prepared to have a magnetic response solely parallel to the orientation of the HMSIW hybrid array antenna, i.e., the Y-axis. The dogbone-shaped was realized in the form 'I'-shaped alphabetic letter due to its strong LC resonant along its Y-axis of its surface while being compact to X-axis. Such sumptuous characteristics come from its inherent structural anisotropy, making it suitable for numerous meta-surface-based wireless communication. When the TE_{101} plane wave of HMSIW hybrid array hits the 3×3 array of meta-surface, in Fig. 4.19(b), at normal. Fig. 4.20 imparts the proposed meta-surface magnetic response, which shows in-phase reflection around at 2.42GHz. The BW of the meta-surface can be identified from 2.39GHz to 2.49GHz; within this band, the meta-surface is supposed to provide constructive interference to the TE_{101} wave.

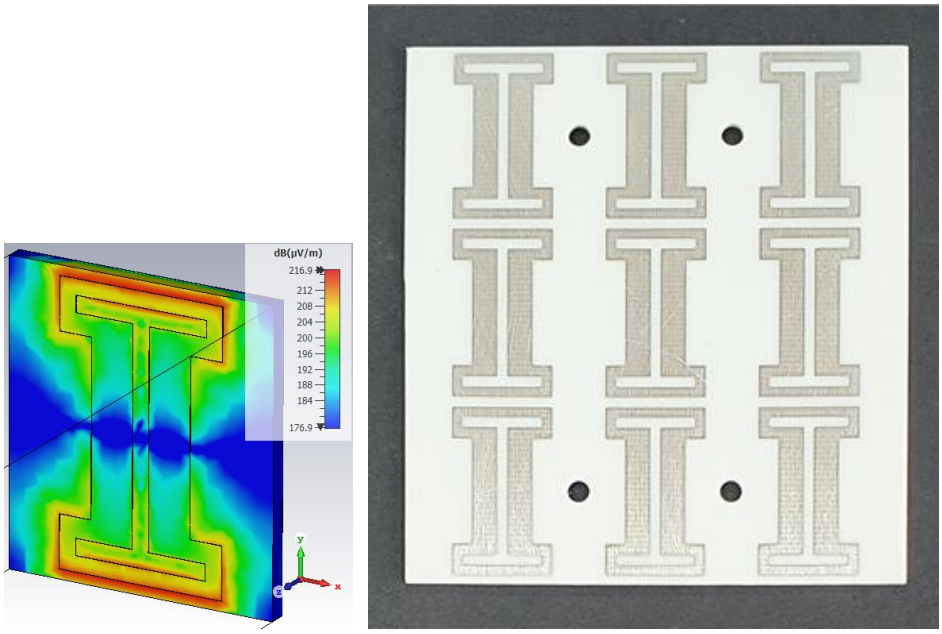

(a) (b)

Fig. 4. 19. (a) single unit cell and (b) photograph of the fabricated 3 × 3 array of artificial magnetic conductor.

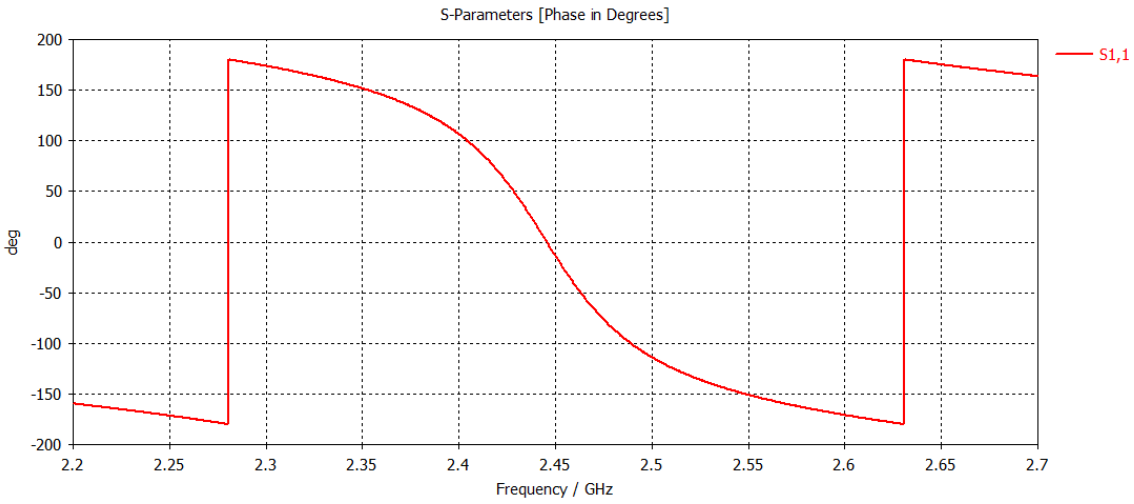

Fig. 4.20. The magnetic response of the proposed artificial magnetic conductor over its operating frequency.

TABLE 4.2: COMPARISON OF BOTH THE MEASURED AND SIMULATED DATA FOR THE CASE-III ANTENNA

	S_{11} (dB)	BW	Realized gain (dBi)	SLL (dBi)	XPL	FTBR
Simulated (13.38 GHz)	-31.0	330 MHz	4.17 (E) 8.51 (H)	-8.10 (E) -7.50 (H)	-14.1 (E) -17.7 (H)	12.85
Measured (13.32 GHz)	-45.9	490 MHz	3.90 7.97	-7.25 (E) -5.0 (H)	-11.4 (E) -13.2 (H)	12.0

4.6 COMPARISON AND DISCUSSION

Table 4.3 is proposed to dish out a comparison with previously published work. In Table 4.3, λ_0 denotes free-space wavelength, and ML stand for microstrip line. Compared with a compact multiband quarter-mode SIW antenna [19], the proposed hybrid array antenna has a higher gain. The employment of a thicker substrate results in a wide percentage BW of the antenna in [19]. Besides, comparing the reported performance of the SIW antenna [44] operating at X, Ku-band reveals the proposed antenna in this article offers both a higher gain and higher BW while being compact. Additionally, the proposed antenna has elevated gain compared to an antenna in [45]. Clearly, the antenna in [45] employed probe feed, making fabrication a bit tougher and integrating with the planner circuit more complex. Furthermore, the employment of a thicker substrate [45] causes wider BW, which inversely also increases XPL. Obviously, the proposed hybrid antenna's thickness, in this article, is more compact and has achieved well over gain compared to the antenna in [43]. After all, the proposed hybrid antenna shows an improvement in gain compared with the previously published one in [33], while both antennas are nearly compact. Antenna in [33] has a wide BW than proposed antenna in this thesis, it is because, in this thesis, BW is sacrificed to achieve high gain.

TABLE 4.3: PERFORMANCE COMPARISON WITH PREVIOUSLY PUBLISHED ANTENNA

Ref. []	**Parameters**					
	Thickness	ε_r	**Gain (dBi)**	**BW (%)**	**Freq. band**	**feed**
[19]	0.02 λ_0 (1.57mm)	2.22	4.1/7.1/6	NM/23.12	C, X, Ku	ML
[43]	0.05 λ_0 (1.57mm)	2.22	4.8/6.1	1.4/5.9	X, Ku	SIW, ML
[44]	0.02 λ_0 (0.787mm)	2.22	5.3/4.3	2.02/1/46	X, Ku	ML
[45]	0.06 λ_0 (1.524mm)	2.22	7.4	4.2	Ku	Probe
[33]	0.02 λ_0 (0.787mm)	2.22	7.5	10	C	ML
This work	0.03 λ_0 (0.812mm)	3.55	8	3.7	Ku	ML

.

Chapter 5: CONCLUSIONS

5.1 GENERAL

In this thesis work, a high gain array antenna with planar SIW technique is presented. The fundamental concept of MPA is used to design the proposed antenna. The successful integration of both patch and cavity-backed antenna allows BW enhancement. Further dividing of the patches allow gain enhancement.

The fundamental parameters of an antenna are discussed in chapter 2 where the up and down sides of the MPA is also mentioned. Antennas feeding technique and polarization details are presented in this chapter. The rectangular waveguide and SIW and their passive circuits are well discussed in this chapter. This chapter gives an in-depth idea about, rectangular and planner SIW, MPA and their structure, parameters and characteristics.

In chapter 3, a couple of cavity-backed hybrid array antennas have been proposed and tested one of them. The exhaustive analysis of numerous parameters is done with the help of the CST studio suite, and experimental data are compared with HFSS too. HMSIW technique allows the antenna to have a small size. It offers the antenna to be installable in the planner circuitry, providing the same radiation performance as a conventional metallic cavity, high gain, and better polarization purity with flexibility. The proposed article shows that integrating a patch improves antenna BW. Most importantly, it also shows that further division of the patch into several small resonators elevates antenna performances. Multi-resonators technique and array scheme have been applied here to promote its characteristics behaviour in its operating range. In addition, the measured results agree well with simulated data and validate the theoretical

analysis presented in this article. A proposed comparison table implies advancement in the gain of around 8.0 dBi compared to previously published work. Besides, the antenna's other parameters are in the satisfying range, making the antenna suitable for wireless communication in IEEE Ku-band. In addition, the employment of an artificial magnetic conductor with this hybrid antenna will improve antenna performance in its operating range.

5.2 LIMITATIONS AND RECOMMENDATION FOR FURTHER STUDY

Obviously, two proposed array antennas can be further advanced to increase their impact on the communications applications. Some of the features that have been identified during this work to be worth further study are discussed below:

- **Meta-surface (artificial magnetic conductor):** The proposed hybrid antenna in chapter 4 has achieved a high gain of 8.0dBi and wide BW behavior of 490 MHz after merging two different frequencies. However, meta-surface (MS) can be employed to achieve better response from the hybrid antenna. Since the patch is divided into more pieces, it would be more reasonable to use the meta-surface concept for this sub array loaded cavity antenna [67].
- **Impedance Bandwidth:** The proposed array antenna in chapter 3 is based on the concept of SIW's. As a result, they suffer from narrow bandwidth as they have vias which contributes to inductance. However, it is considered that many of the state-of-the-art methods for decreasing the *Q*-factor (hence increasing bandwidth) are also applicable to the proposed SIW antennas. Bandwidth can be increased by using special techniques such as selection of suitable patch shape, selection of suitable feeding technique, multimode techniques, thicker substrate, embedding meta-materials etc. Generally low permittivity and increased substrate thickness lead to superior performance (better efficiency, greater bandwidth, higher directivity).

- **Miniaturization:** SIW antennas can be miniatured according to the magnetic wall of their fundamental frequency. In this way, half, quarter, and even eighth mode is possible to achieve. By doing so, the antenna size can be reduced further and can be made superior to the planar circuit. In this chapter 4, antenna employs the half-mode technique. However, by using quarter-mode technique, antenna size can be reduced further for future wireless applications.
- **Feed line:** The array antenna of chapter 4 employs a feed line that is on the obverse side of the substrate. As a result, its radiation could harm the radiation from the main antenna resulting in a degradation of the antenna's main radiation. Therefore, by placing the feed line on the rear side, radiation can be improved further by effectively suppressing secondary waves and can escalate gain along with better directivity.

REFERENCES

[1] A. H. Murshed, M. A. Hossain, E. Nishiyama, and I. Toyoda, "Design and characterization of frequency reconfigurable honey bee antenna for cognitive radio application," Int. J. Electr. Comput. Eng., vol. 12, no. 6, pp. 6178–6186, Dec. 2022.

[2] A. H. Murshed, M. A. Hossain, M. A. Rahman, E. Nishiyama, and I. Toyoda, "Designing of a both-sided MIC starfish microstrip array antenna for K-band application," in Proc. IEEE Region 10 Symp., Aug. 2021, pp. 1–6.2016.

[3] A. H. Murshed, M. A. Hossain, M. A. Rahman, E. Nishiyama, and I. Toyoda, "Design and characterization of polarization reconfigurable heart shape monopole antenna for 2.4 GHz application," Int. J. Electr. Comput. Eng., vol. 12, no. 4, pp. 3808–3819, Aug. 2022.

[4] M. A. Hossain, A. H. Murshed, M. A. Rahman, E. Nishiyama, and I. Toyoda, "A gain enhanced linear polarization switchable array antenna with switching diodes," Int. J. RF Microw. Comput.-Aided Eng., vol. 32, no. 10, pp. 1–9, Jun. 2022.

[5] I. Rosaline, A. Kumar, P. Upadhyay, and A. H. Murshed, "Four element MIMO antenna systems with decoupling lines for high-speed 5G wireless data communication," Int. J. Antennas Propag., vol. 2022, pp. 1–13, Jun. 2022

[6] Q. Y. Liu, Z. Shen, and C. L. Law, "A compact dual-band cavity-backed slot antenna," IEEE Antennas Wireless Propag. Lett., vol. 5, pp. 4–6, 2006

[7] W. Hong, N. Behdad, and K. Sarabandi, "Size reduction of cavity-backed slot antennas," IEEE Trans. Antennas Propag., vol. 54, no. 5, pp. 1461–1466, May 2006..

[8] N. C. Karmakar, "Investigations into a cavity-backed circularpatch antenna," IEEE Trans. Antennas Propag., vol. 50, no. 12, pp. 1706–1715, Dec. 2002.

[9] F. Xu and K. Wu, "Guided-wave and leakage characteristics of substrate integrated waveguide," IEEE Trans. Microw. Theory Techn., vol. 53, no. 1, pp. 66–73, Jan. 2005.

[10] G. Q. Luo, Z. F. Hu, L. X. Dong, and L. L. Sun, "Planar slot antenna backed by substrate integrated waveguide cavity," IEEE Antennas Wireless Propag. Lett., vol. 7, pp. 236–239, 2008.

[11] J. C. Bohorquez, H. A. F. Pedraza, I. C. H. Pinzon, J. A. Castiblanco, N. Pena, and H. F. Guarnizo, "Planar substrate integrated waveguide cavity-backed antenna," IEEE Antennas Wireless Propag. Lett., vol. 8, pp. 1139–1142, 2009.

[12] C. A. T. Martinez, J. C. B. Reyes, O. A. N. Manosalva, and N. M. P. Traslavina, "Volume reduction of planar substrate integrated waveguide cavity-backed

antennas," in Proc. 6th Eur. Conf. Antennas Propag. (EUCAP), Mar. 2012, pp. 2919–2923.

[13] S. A. Razavi and M. H. Neshati, "Development of a linearly polarized cavity-backed antenna using HMSIW technique," IEEE Antennas Wireless Propag. Lett., vol. 11, pp. 1307–1310, 2012.

[14] B. Liu, W. Hong, Y.-Q. Wang, Q.-H. Lai, and K. Wu, "Half mode substrate integrated waveguide (HMSIW) 3-dB coupler," IEEE Microw. Wireless Compon. Lett., vol. 17, no. 1, pp. 22–24, Jan. 2007.

[15] F. Ben, J. G. D. K. David Burns, M. P. L. Samin, and S. Peirovi, "Demand Response and Advanced Metering," *Federal Energy Regulatory Commission, USA*, 2017.

[16] Q. H. Lai, W. Hong, Z. Q. Kuai, Y. S. Zhang, and K. Wu, "Halfmode substrate integrated waveguide transverse slot array antennas," IEEE Trans. Antennas Propag., vol. 57, no. 4, pp. 1064–1072, Apr. 2009.

[17] G. M. Zelinski, G. A. Thiele, M. L. Hastriter, M. J. Havrilla, and A. J. Terzuoli, "Half width leaky wave antennas," IET Microw., Antennas Propag., vol. 1, no. 2, pp. 341–348, Apr. 2007.

[18] A. J. Martinez-Ros, J. L. Gomez-Tornero, and G. Goussetis, "Planar leaky-wave antenna with flexible control of the complex propagation constant," IEEE Trans. Antennas Propag., vol. 60, no. 3, pp. 1625–1630, Mar. 2012.

[19] C. Jin, R. Li, A. Alphones, and X. Bao, "Quarter-mode substrate integrated waveguide and its application to antennas design," IEEE Trans. Antennas Propag., vol. 61, no. 6, pp. 2008–2921, Jun. 2013.

[20] Z. Z. Chen, W. Hong, Z. Kuai, J. Chen, and K. Wu, "Circularly polarized slot array antenna based on substrate integrated waveguide," in Proc. Int. Conf. Microw. Millim. Wave Technol., vol. 3, Apr. 2008, pp. 1066–1069.

[21] M. H. Awida and A. E. Fathy, "Substrate-integrated Ku-band cavitybacked 2 × 2 microstrip patch array antenna," IEEE Antennas Wireless Propag. Lett., vol. 8, pp. 1054–1056, 2009.

[22] M. H. Awida, S. H. Suleiman, and A. E. Fathy, "Substrate-integrated cavity-backed patch arrays: A low-cost approach for bandwidth enhancement," IEEE Trans. Antennas Propag., vol. 59, no. 4, pp. 1155–1163, Apr. 2011.

[23] W. Sang-Hyuk, L. Yong-Shik, and Y. Jong-Gwan, "Wideband microstrip match antenna with U-shaped parasitic elements," IEEE Trans. Antennas Propag., vol. 55, no. 4, pp. 1196–1199, Apr. 2007.

[24] J. S. Egashira and E. Nishiyama, "Stacked microstrip antenna with wide bandwidth and high gain," IEEE Trans. Antennas Propag., vol. 44, no. 11, pp. 1533–1534, Nov. 1996.

[25] J. E. Nishiyama and M. Aikawa, "Wide-band and high-gain microstrip antenna with thick parasitic patch substrate," in Proc. IEEE Antennas Propag. Soc. Int.

Symp. (APSURSI), vol. 1, Jun. 2004, pp. 273–276.

[26] T. Seki, K. Nishikawa, I. Toyoda, and S. Kubota, "Microstrip array antenna with parasitic elements alternately arranged over two layers of LTCC substrate for millimeter wave applications," in Proc. IEEE Radio Wireless Symp., Jan. 2007, pp. 149–152.

[27] S. F. H. Lin and Z. N. Chen, "A method of suppressing higher order modes for improving radiation performance of metasurface multiport antennas using characteristic mode analysis," IEEE Trans. Antennas Propag., vol. 66, no. 4, pp. 1894–1902, Apr. 2018.

[28] F. H. Lin and Z. N. Chen, "Truncated impedance sheet model for lowprofile broadband nonresonant-cell metasurface antennas using characteristic mode analysis," IEEE Trans. Antennas Propag., vol. 66, no. 10, pp. 5043–5051, Oct. 2018.

[29] F. Xu, K. Wu, and X. Zhang, "Periodic leaky-wave antenna for millimeter wave applications based on substrate integrated waveguide," IEEE Trans. Antennas Propag., vol. 58, no. 2, pp. 340–347, Feb. 2010.

[30] L. Yan, W. Hong, G. Hua, J. Chen, K. Wu, and T. J. Cui, "Simulation and experiment on SIW slot array antennas," IEEE Microw. Wireless Compon. Lett., vol. 14, no. 9, pp. 446–448, Sep. 2004.

[31] C. Jin, A. Alphones, and L. C. Ong, "Broadband leaky-wave antenna based on composite right/left handed substrate integrated waveguide," Electron. Lett., vol. 46, no. 24, pp. 1584–1585, Nov. 2010.

[32] C. Jin and A. Alphones, "Leaky-wave radiation behavior from a double periodic composite right/left-handed substrate integrated waveguide," IEEE Trans. Antennas Propag., vol. 60, no. 4, pp. 1727–1735, Apr. 2012.

[33] H. Dashti and M. H. Neshati, "Development of low-profile patch and semi-circular SIW cavity hybrid antennas," IEEE Trans. Antennas Propag., vol. 62, no. 9, pp. 4481–4488, Sep. 2014.

[34] D. M. Pozar, Microwave Engineering, 3rd ed. New York, NY, USA: Wiley, 2004.

[35] G. Q. Luo, W. Hong, Q. H. Lai, K. Wu, and L. L. Sun, "Design and experimental verification of compact frequency-selective surface with quasi-elliptic bandpass response," IEEE Trans. Microw. Theory Techn., vol. 55, no. 12, pp. 2481–2487, Dec. 2007.

[36] C. A. Balanis, Antenna Theory Analysis and Design. 3rd ed. New York, NY, USA: Wiley, 2005.

[37] A. S. Kaddour, A. Clemente, S. Bories, and C. Delaveaud, "Design of high directivity compact parasitic array for beam-steering applications," in Proc. 9th Eur. Conf. Antennas Propag. (EuCAP), Apr. 2015, pp. 1–5.

[38] J. R. James, P. S. Hall, and C. Wood, Microstrip Antenna Theory and Design (IEE Electromagnetic Wave Series). London, U.K.: Peter Peregrinus Ltd, 1981.

[39] Y. Lo, D. Solomon, and W. Richards, "Theory and experiment on microstrip antennas," IEEE Trans. Antennas Propag., vol. AP-27, no. 2, pp. 137–145, Mar. 1979.

[40] A. P. Feresidis, G. Goussetis, S. Wang, and J. C. Vardaxoglou, "Artificial magnetic conductor surfaces and their application to low-profile highgain planar antennas," IEEE Trans. Antennas Propag., vol. 53, no. 1, pp. 209–215, Jan. 2005.

[41] W. Huang, J.-X. Du, G.-N. Tan, and X.-X. Yang, "A novel 35-GHz slot-coupled patch rectenna array based on SIW cavity for WPT," in Proc. Int. Conf. Microw. Millim. Wave Technol. (ICMMT), May 2019, pp. 1–3.

[42] J. M. I. Alonso, G. A. Calderón, and M. S. Pérez, "SIW antenna with polarizer at Ku-band," IEEE Trans. Antennas Propag., vol. 63, no. 6, pp. 2782–2786, Jun. 2015.

[43] T. Zhang, W. Hong, Y. Zhang, and K. Wu, "Design and analysis of SIW cavity backed dual-band antennas with a dual-mode triangular-ring slot," IEEE Trans. Antennas Propag., vol. 62, no. 10, pp. 5007–5016, Oct. 2014.

[44] S. Mukherjee, A. Biswas, and K. V. Srivastava, "Substrate integrated waveguide cavity-backed dumbbell-shaped slot antenna for dual frequency applications," IEEE Antennas Wireless Propag. Lett., vol. 14, pp. 1314–1317, 2015.

[45] T. Liang, Z. Wang, and Y. Dong, "A circularly polarized SIW slot antenna based on high-order dual-mode cavity," IEEE Antennas Wireless Propag. Lett., vol. 19, no. 3, pp. 388–392, Mar. 2020.

[46] IEEE, "IEEE Standard Definitions of Terms for Antennas," IEEE, pp. 0-1, February 1983 [Online]. http://ieeexplore.ieee.org/stamp/stamp.jsp?tp=&arnumber=30651&isnumber=1290 [Accessed May 03, 2023].

[47] Lee, K.F., and Chen, W.: 'Advances in microstrip and printed antennas' (John Wiley & Sons, Inc., 1997).

[48] C. A. Balanis, Antenna theory: Analysis and design, John Wiley and Sons Inc., 1997.

[49] C. Hu, J. Wang, W. Tian, T. Zeng, and R. Wang, "Design and imaging of ground-based multiple-input multiple-output synthetic aperture radar (MIMO SAR) with non-collinear arrays," Sensors, vol. 17, no. 3, 2017.

[50] Tutorials Point, Antenna Theory-Beam Width, [online] https://www.tutorialspoint.com/antenna_theory/antenna_theory-_beam_width.htm [Accessed May 07 2023].

[51] G. A. Deschamps, "Microstrip microwave antennas," in proceedings of the 3rd USAF symposium on antennas, 1953.

[52] P. Bhartia, K. V. S. Rao and R. S. Tomar, Millimeter-wave microstrip and printed circuit antennas, Artech House, Norwood, MA, 1991.

[53] Y. Lo, D. Solomon, and W. Richards, “Theory and experiment on microstrip antennas,” IEEE Trans. Antennas Propag., vol. AP-27, no. 2, pp. 137–145, Mar. 1979.

[54] “Inverted-F Antenna” [online] https://en.wikipedia.org/wiki/Inverted-F_antenna [Accessed June 08, 2023].

[55] G. Luo, Qing and L. Sun. “Circularly polarized antenna based on dual-mode circular SIW cavity.” 2008 International Conference on Microwave and Millimeter Wave Technology, vol. 3, pp. 1077- 1079, 2008.

[56] "Vivaldi Antenna” [online] https://en.wikipedia.org/wiki/Vivaldi_antenna [Accessed June 08, 2023].

[57] T. Zhang, W. Hong, Y. Zhang, and K. Wu, “Design and analysis of SIW cavity backed dual-band antennas with a dual-mode triangular-ring slot,” IEEE Trans. Antennas Propag., vol. 62, no. 10, pp. 5007–5016, Oct. 2014.

[58] David M. Pozar, Microwave Engineering, 2nd edition, John Wiley & Sons, Inc., 1998.

[59] “Circular Polarization” [online] http://hyperphysics.phy-astr.gsu.edu/hbase/phyopt/polclas.html [Accessed May June 01, 2022]

[60] E. O. Hammerstad, “Equations for microstrip circuit design,” 5th European Microwave Conf., pp. 2268-272, 1975.

[61] D. Pozar, Microwave Engineering, 3rd ed. John Wiley & Sons, 2005.

[62] T.-Y. Huang, T.-M. Shen, and R.-B. Wu, “Design and modeling of microstrip line to substrate integrated waveguide transitions,” Passive Microwave Components and Antennas, Apr 2010.

[63] M. B. R. Garg, I. Bahl, Microstrip Lines and Slotlines, 3rd ed. Artech House, 2013.

[64] C. Hu, J. Wang, W. Tian, T. Zeng, and R. Wang, “Design and imaging of ground-based multiple-input multiple-output synthetic aperture radar (MIMO SAR) with non-collinear arrays,” Sensors, vol. 17, no. 3, 2017.

[65] A. A. R. Saad, W. M. Hassan, A. A. Ibrahim, “A monopole antenna with cotton fabric material for wearable applications” scientific reports, vol. 13, pp. 73135, 2023.

[66] "Institute of Electronics" [online]

https: http://www.eletel.p.lodz.pl/eng/index.php/artificial-magnetic-conductor-amc [Accesses 06 August 2023]

[67] X. Yang, J. Hu, Y. Ji, and L. Ge, and X. Zeng "Design of a Metasurface Antenna with Pattern Diversity," IEEE Antenna and Propag. Lett, vol. 19, no. 12, pp. 2467-2471, Dec. 2020.